Earth Planet. Sci. Lett. 646 (2024) 118980

Contents lists available at ScienceDirect

Earth and Planetary Science Letters

journal homepage: www.elsevier.com/locate/epsl

Vertical transport of anthropogenic lead by reversible scavenging in the South Atlantic Ocean

Arianna Olivelli [a,b,*], Maxence Paul [b], Hui Xu [b], Katharina Kreissig [b], Barry J. Coles [b], Rebekah E.T. Moore [b], Luke Bridgestock [c], Micha Rijkenberg [d], Rob Middag [d,e], Maeve C. Lohan [f], Dominik J. Weiss [b], Mark Rehkämper [b], Tina van de Flierdt [b]

[a] Grantham Institute for Climate Change and the Environment, Imperial College London, South Kensington Campus, London SW7 2AZ, United Kingdom
[b] Department of Earth Science and Engineering, Imperial College London, South Kensington Campus, London SW7 2AZ, United Kingdom
[c] School of Earth and Environmental Sciences, University of St Andrews, Bute Building, Queen's Terrace, St Andrews, KY16 9TS, United Kingdom
[d] NIOZ Royal Netherlands Institute for Sea Research, Department of Ocean Systems, PO Box 59, 1790 AB Den Burg, the Netherlands
[e] Centre for Isotope Research - Oceans, University of Groningen, PO Box 72, 9700 AB Groningen, the Netherlands
[f] Ocean and Earth Sciences, National Oceanography Centre, University of Southampton, Southampton SO14 3ZH, United Kingdom

ARTICLE INFO

Editor: Prof A Jacobson

Keywords:
Lead isotopes
Scavenging
Seawater
Pollution
GEOTRACES

ABSTRACT

Stable lead (Pb) isotopes have been regarded as tracers of ocean circulation, both in the present time and geological past. Here we present a new dataset of seawater Pb concentrations and isotope compositions for ten depth profiles from the South Atlantic Ocean (GEOTRACES cruises GA02 and GA10). By comparing Pb isotope data collected on the two cruises, and by modelling the distribution of Pb with an extended optimum multi-parameter analysis, we find evidence of vertical transport of anthropogenic Pb pollution due to reversible scavenging. Surface to depth transfer of polluted Pb is aided by high suspended particulate matter loads at the Brazil – Malvinas Confluence and along ~40°S in the South Atlantic. Overall, our findings caution the use of Pb isotope ratios as ventilation tracers in the South Atlantic and emphasize the importance of particle-seawater interaction for biogeochemical cycles.

1. Introduction

Lead (Pb) is a heavy metal that naturally occurs in the environment at trace levels. However, anthropogenic activities, such as the use of leaded gasoline, waste incineration, coal combustion, and non-ferrous metal smelting, have been the main sources of Pb to the ocean since the late 19th century, increasing its concentration levels in the marine environment (e.g., Komárek et al., 2008; Pacyna & Pacyna, 2001). Lead inputs to the global ocean represent one of the "global geophysical experiments" that humankind has performed on Earth (Boyle et al., 2014), as the natural state of the ocean has been altered without knowing the consequences.

Sources of Pb to the marine environment, both natural and anthropogenic, can be differentiated based on their Pb isotope compositions. In open ocean surface waters, Pb is primarily sourced from the atmosphere via deposition of aerosols derived from the continents. Lead in surface waters of the South Atlantic Ocean is predominantly of anthropogenic origin, despite a significant decrease in Pb concentrations between the 1990s and 2011 driven by the ban of leaded gasoline in South American countries (Olivelli et al., 2023).

The residence time of Pb in the surface ocean is approximately 1–10 years, while in intermediate and deep waters it is ~50–100 years (Bacon et al., 1976; Craig et al., 1973; Henderson & Maier-Reimer, 2002; Rigaud et al., 2015). Lead is removed from seawater by scavenging, the abiotic adsorption of dissolved Pb to reactive surfaces of sinking particles. As the residence time of Pb in the deep ocean is much shorter than the deep ocean's mixing time (~ 1000 years) and there is no evidence of significant Pb isotope fractionation during scavenging, stable Pb isotope ratios have been regarded as conservative tracers of water mass movements in the pre-anthropogenic ocean and as transient tracers of ocean ventilation in the modern era (e.g., Bridgestock et al., 2018; Frank, 2002; Henderson & Maier-Reimer, 2002; Véron et al., 1998, 1999).

In their study on natural Pb isotopes as tracers of ocean circulation, Henderson & Maier-Reimer (2002) assumed that scavenging of Pb is an

* Corresponding author.
E-mail address: a.olivelli21@imperial.ac.uk (A. Olivelli).

https://doi.org/10.1016/j.epsl.2024.118980
Received 21 December 2023; Received in revised form 14 August 2024; Accepted 28 August 2024
Available online 19 September 2024

irreversible process, in agreement with the majority of the ^{210}Pb data published at that time (e.g., Bacon et al., 1976; Chung & Craig, 1983; Nozaki et al., 1976). This assumption proved effective in reconstructing the distribution of natural Pb in the ocean in the absence of any anthropogenic sources.

However, anthropogenic inputs have severely perturbed the biogeochemical cycle of Pb in the ocean (Boyle et al., 2014) and need to be accounted for when assessing the use of Pb isotope ratios as tracers of ocean circulation and ventilation. Furthermore, due to different natural abundances in the continental crust and marine environment, discrepancies may arise between the cycling of elemental Pb and radioactive ^{210}Pb. Therefore, caution must be exercised when inferences about the biogeochemical cycling of stable Pb isotopes are derived from studies of the radioactive ^{210}Pb isotope system. Additional investigations that focus on the cycling of Pb and its stable isotopes are therefore deemed necessary (Chen et al., 2016).

Recent studies have highlighted that Pb scavenging in the ocean is likely a two-way process, where dissolved Pb continually re-equilibrates with Pb adsorbed onto sinking particles (Chen et al., 2016; Lanning et al., 2023). This process, termed reversible scavenging, acts to redistribute dissolved Pb vertically within the water column and has implications for interpreting marine Pb distributions solely in terms of ocean circulation and ventilation. Based on measurements of dissolved, colloidal and particulate Pb concentrations and dissolved Pb isotope compositions, reversible scavenging has been identified as the mechanism responsible for the vertical transfer of anthropogenic Pb to deep waters of North Pacific Ocean in areas of high suspended particle matter (SPM) load (Lanning et al., 2023). Whilst such vertical transport of Pb was previously hypothesised to be important (Wu et al., 2010), the study of Lanning et al. (2023) was the first to provide direct evidence for this process in the open ocean.

It has long been accepted that the mechanism of reversible scavenging plays a key role in the marine distribution of highly particle-reactive elements such as Th (Bacon & Anderson, 1982; Honeyman & Santschi, 1989). Whilst studies of stable Pb isotopes argued that the concentrations of elemental Pb are seawater is too low for the formation of secondary Pb minerals by precipitation and that Pb release from decaying organic matter is low, as Pb is not a nutrient (Chen et al., 2016; Lanning et al., 2023), the literature on ^{210}Pb discussed remineralization as a reversible scavenging pathway for Pb (Niedermiller & Baskaran, 2019), as well as adsorption and desorption processes (Nozaki et al., 1997; Sherrell et al., 1992).

Following on from the study of Lanning et al. (2023), we hypothesise that other ocean areas where SPM loads are high, like the Brazil – Malvinas Confluence in the South Atlantic, might be subject to vertical transport of anthropogenic Pb. In contrast to the sluggish circulation in the North Pacific, the Atlantic is a highly advective ocean basin, characterised by strong transport of water at all depths as part of the Atlantic Meridional Overturning Circulation. The South Atlantic, featuring water masses forming both in the Atlantic sector of the Southern Ocean and in the North Atlantic Ocean, is hence an ideal location to test the hypothesis that vertical transport of Pb by reversible scavenging might regionally alter and dominate the advected Pb isotope signal.

In this study, we present and analyse new Pb concentration and isotope data for 10 depth profiles from two GEOTRACES cruises, namely GA02 (Leg 3) and GA10, to identify the major processes that drive the distribution of Pb concentrations and isotope compositions in the South Atlantic Ocean. Moreover, we question and assess the robustness of Pb isotopes as water mass and ventilation tracers in areas where reversible scavenging might alter the advected Pb isotope signal.

2. Methods

2.1. Seawater sampling

Depth profiles for seawater Pb isotope compositions and concentrations were collected during two GEOTRACES sections in the South Atlantic between 2010 and 2012 (Fig. 1). In detail, 40 samples from four different stations were collected on the *RRS James Cook* (JC057) during Leg 3 of GEOTRACES section GA02 between 2nd March and 6th April 2011. In addition, six different stations were sampled during the two legs of GEOTRACES GA10, in October - November 2010 on the *RSS Discovery* (D357), and in December 2011 to January 2012 on the *RRS James Cook* (JC068). All samples were collected unfiltered from ultra clean CTD bottles into pre-cleaned 1 L HDPE bottles, acidified to pH ~2.1 with 2 mL L^{-1} distilled 6 M HCl, sealed with parafilm and double bagged to avoid contamination. Prior to analysis, samples collected on cruise GA02 were further acidified to pH 1.7 ± 0.1 with distilled 6 M HCl and left to equilibrate for at least six days before processing, as they were analysed 11 years after collection. This was not the case for GA10 samples which were analysed less than three years from collection.

All samples represent total dissolvable Pb (TDPb), encompassing Pb within the dissolved (<0.2 μm) pool in addition to easily leachable Pb (LpPb) from suspended particulate matter within seawater. For most open ocean seawater samples, the latter provides only minor contributions to total dissolvable Pb budgets but can be important close to continental margins (e.g., Bridgestock et al., 2018; Olivelli et al., 2023; Schlosser et al., 2019). Dissolved Pb (DPb) concentrations for these samples were measured by other groups and are reported in the GEOTRACES Intermediate Data Product (2021). A thorough assessment of the contribution of LpPb to the TDPb concentrations and isotope compositions measured in this study is available in SI Note 1. Briefly, the average LpPb contribution to TDPb concentrations is 20 % for GA02 samples and 24 % for GA10 samples, and the measured TDPb isotope compositions are largely reflective of the DPb isotope compositions of the seawater samples. In the following sections, concentration and isotope composition data refer to TDPb unless specified as DPb.

2.2. Analytical techniques

All laboratory work took place in the ISO class 6 clean rooms and the mass spectrometry facilities of the MAGIC Laboratories at Imperial College London.

2.2.1. Lead isotope compositions

2.2.1.1. Nobias chelate PA-1 resin and MC-ICP-MS. The Pb isotope compositions of GA02 samples were determined following the methodology of Griffiths et al. (2020). In brief, 1.5–1.9 L of seawater were used to pre-concentrate and separate Pb for isotopic analysis using the Nobias Chelate PA-1 resin and anion exchange chromatography (Table S1). The Pb eluted in the final step of chromatography was split in two aliquots: 1/3 of it was spiked with a ^{204}Pb–^{207}Pb double spike, and the remaining 2/3 were left unspiked. Both aliquots were doped with a solution of NIST Standard Reference Material (SRM) 997 Tl to obtain an elemental ratio of Pb:Tl of 1:3 to enable correction of the measured Pb isotope ratios for instrumental mass bias (Woodhead, 2002). Samples were analysed on a Nu Plasma II multi-collector inductively coupled plasma mass spectrometer (MC-ICP-MS). All Faraday cups were equipped with 10^{11} Ω resistors, except the two cups monitoring ^{201}Hg and ^{204}Pb+^{204}Hg, which were equipped with 10^{12} Ω resistors to improve the precision of the measurements of the Pb isotope ratios encompassing the minor ^{204}Pb isotope. The data acquired in the analyses of the spiked and unspiked aliquots were processed offline to correct the Pb isotope ratios for instrumental mass bias using the double spike technique (Griffiths et al., 2020; Rudge et al., 2009).

Procedural blanks were determined by processing twice a single 1 L aliquot of 'Pb-free seawater', obtained by stripping seawater of Pb with five cycles of Nobias resin extraction. The long-term blank for all sample batches was 12 ± 9 pg Pb (n = 5, 1SD), equivalent to an average of 0.3 %

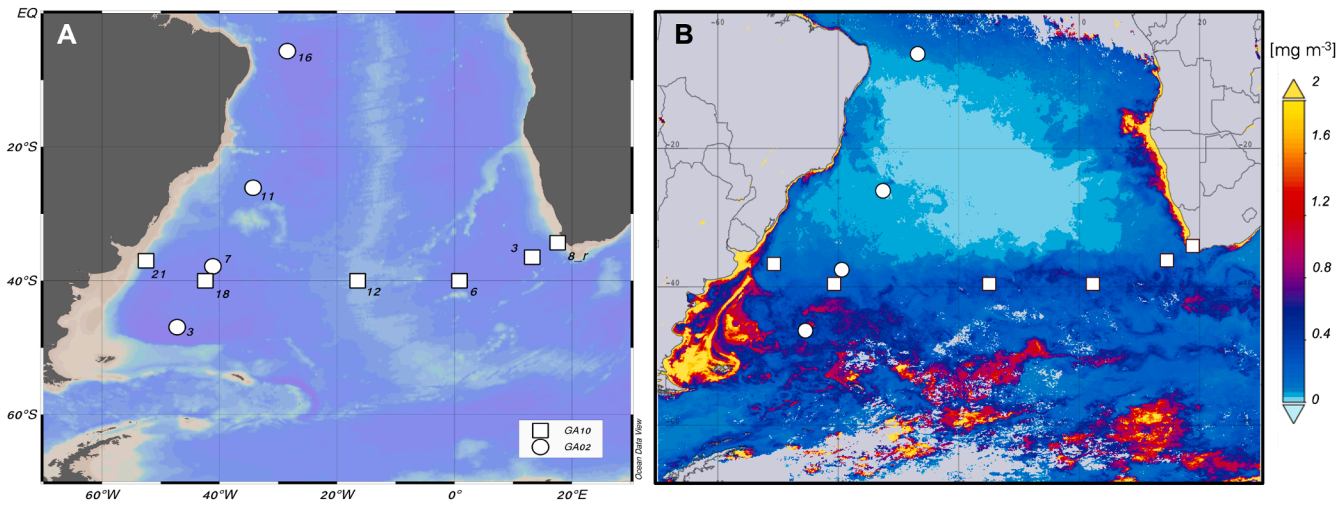

Fig. 1. South Atlantic Ocean sampling locations for Pb isotopes and concentrations on GEOTRACES cruises GA02 Leg 3 (circles) and GA10 (squares). Corresponding Station numbers are reported next to each symbol in panel A. Background: A) Bathymetry; B) Monthly averaged surface chlorophyll-a concentrations [mg m^{-3}] in January 2012. Background visualisation for panel B produced using the GIOVANNI online data system and MODIS-Aqua data.

of the total Pb available for the isotope measurements (4.8 ± 1.5 ng Pb, n = 40, 1SD). As the Pb blank for the samples was essentially negligible and the blank isotope composition was variable, no blank correction was performed for the Pb isotope data of samples.

2.2.1.2. Co-precipitation with $Mg(OH)_2$ and tims. The Pb isotope compositions of the GA10 samples were determined following the methodology of Paul et al. (2015a). Briefly, up to 2 L of seawater were used to pre-concentrate and separate Pb by co-precipitation with $Mg(OH)_2$ and anion exchange chromatography (Table S1). Akin to the procedure followed for GA02 samples, the Pb eluted from the final step of the chromatography procedure was split in two parts (1/3 spiked, 2/3 unspiked) before being loaded onto *Re* filaments with silica gel activator. The samples were measured on a Triton thermal ionisation mass spectrometer (TIMS), using Faraday cups fitted with 10^{11} Ω resistors. The measured data for spiked and unspiked runs of each sample were processed using an iterative double spike data reduction routine to correct for instrumental mass fractionation (Rudge et al., 2009).

Procedural blanks were determined by carrying out the entire analytical procedure in absence of an initial seawater sample. Overall, the mean long-term blank was 28 ± 21 pg Pb (1SD, n = 25). Like the analyses of the GA02 samples, the blank contributes only 0.1–2.5 % to the indigenous Pb analysed in the samples and its isotopic composition was variable between analytical days (see Paul et al. (2015a) for details). Therefore, no blank correction was applied to the measured Pb isotope data.

2.2.2. Lead concentrations

Lead concentrations for samples from both cruises were determined using the isotope dilution (ID) method developed by Paul et al. (2015a). Briefly, 50 ml of seawater were spiked with the same ^{204}Pb–^{207}Pb mixture used for isotope composition measurements and left to equilibrate for at least 10 days. After equilibration, Pb was pre-concentrated by co-precipitation with $Mg(OH)_2$ and separated from the matrix by anion exchange chromatography (Table S2). Samples were measured on a Nu Plasma II MC-ICP-MS (GA02) or a Triton TIMS instrument (GA10).

All Pb concentrations were corrected by subtracting the mean blank value obtained for either each analytical day (GA02; as blank values varied notably between analytical days) or the mean blank value of the session (GA10). For GA02 samples, blank contributions were determined following the ID procedure using 200 µl of 'Pb-free seawater' (obtained as described above). The average blank value for all batches was 11.5 ± 12.8 pg Pb (1SD, n = 25, ranging between 2.4 and 53.6 pg Pb, with the latter being an exceptionally high value). For GA10 samples, blank contributions were determined using 100 µl of seawater (containing negligible amounts of Pb, ~0.2 – 1 pg), and the average value was 11.7 ± 4.3 pg Pb (1SD, n = 36).

2.2.3. Data quality

The quality of the Pb isotope data was assessed by analysing NIST SRM 981 in quantities varying between 1 and 3 ng Pb. All results were in good agreement with previously published values (Table S3; Galer and Abouchami, 1998; Griffiths et al., 2020; Olivelli et al., 2023). An aliquot of approximately 500 ml of an in-house seawater quality control material with a known Pb concentration of 85.6 pmol/kg was analysed for its Pb isotope composition together with each batch of 10 samples during the GA02 sample analyses. For this sample, the reproducibility (2SD) of the Pb isotope composition was ± 680 ppm (0.068 %) for $^{206}Pb/^{207}Pb$, ± 200 ppm (0.020 %) for $^{208}Pb/^{207}Pb$, and ± 500–760 ppm (0.050–0.076 %) for the minor $^{20x}Pb/^{204}Pb$ ratios. Additionally, GEOTRACES seawater intercalibration samples GSI and GDI were measured in the same analytical session as the GA10 samples and the results agreed with the published reference values (Table S3; Paul et al., 2015a).

3. Hydrography

The hydrography of the two cruise sections has been extensively described in previous publications, both for GA02 (Deng et al., 2014; Dulaquais et al., 2014; Middag et al., 2015, 2018, 2020; Rijkenberg et al., 2014; Xie et al., 2014) and GA10 (Schlosser et al., 2019; Tuerena et al., 2015; Wyatt et al., 2014). A short overview is provided below, as it is relevant for the interpretation of the results.

Both sections sampled all the main water masses of the South Atlantic Ocean (Fig. 2), namely South Atlantic Central Water (SACW), Antarctic Intermediate Water (AAIW), Upper Circumpolar Deep Water (UCDW), North Atlantic Deep Water (NADW) and Antarctic Bottom Water (AABW). Below the mixed layer, SACW occupies depths between 200 and 500 m, and is identified by a wide range of temperatures (4.4 – 17.5 °C) and salinities (34.2 – 35.9), in agreement with previous studies (Stramma and England, 1999). Underneath, AAIW extends between 500 and 1500 m depth, and is identified by a clear salinity minimum (34.2) and a core at $\sigma_\theta = 27.3$ (Talley et al., 2011). Both SACW and AAIW have multiple sources and areas of formation in the South Atlantic Ocean and connected basins. In detail, SACW forms from different subtropical mode waters originating both in the South Atlantic and Indian Ocean,

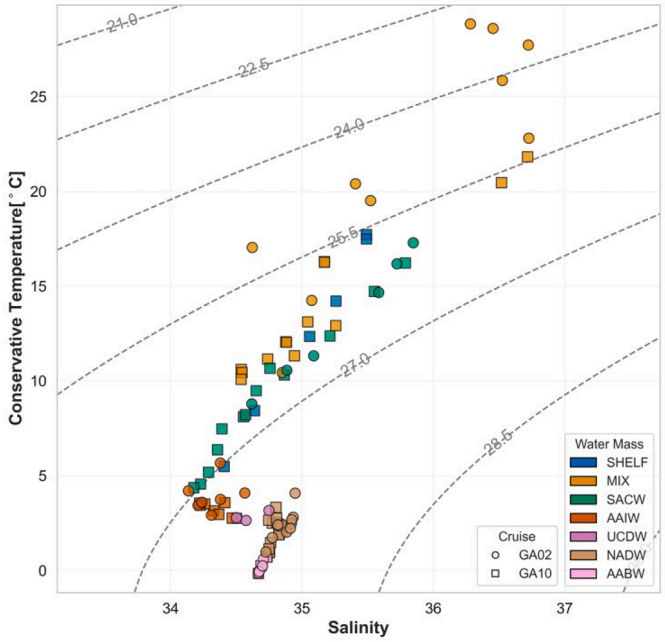

Fig. 2. Temperature-salinity diagram for all GA02 and GA10 samples collected for Pb isotope and concentration analysis. Water masses labels: SHELF – samples from GA10 Station 8_r, located on the shelf off South Africa; MIX – mixed layer; SACW – South Atlantic Central Water; AAIW – Antarctic Intermediate Water; UCDW – Upper Circumpolar Deep Water; NADW – North Atlantic Deep Water; AABW – Antarctic Bottom Water.

the latter transported through the Agulhas leakage (Azar et al., 2021; Poole and Tomczak, 1999; Souza et al., 2018). The exact origin of AAIW, on the other hand, is still debated and both circumpolar and localised areas of formation have been discussed in the literature (Li et al., 2022; Santoso and England, 2004; Xia et al., 2022). Therefore, while samples collected at different latitudes and longitudes in the South Atlantic might belong to the same water mass, the areas where the water last ventilated might be different. Upper Circumpolar Deep Water sits between AAIW and NADW, and is formed as a mixture of AAIW, NADW and shelf water from around Antarctica that is not dense enough to become deep water, with additional influences from the Indian and Pacific Oceans (Orsi et al., 2002; Santoso et al., 2006; Talley et al., 2011). North Atlantic Deep Water is the only water mass encountered in the South Atlantic water column that is ventilated in the Northern Hemisphere. It originates in the high latitudes of the Atlantic Ocean and travels southward preferentially as a deep western boundary current at a core depth of 2500 m. As it travels southward, it progressively mixes with waters generated in the South Atlantic. At 40–45°S, at the location of the South Atlantic Current and north of the Subantarctic Front, NADW flows zonally from the western to the eastern side of the South Atlantic basin (Stramma and England, 1999). Lastly, the northward travelling and very dense AABW is found below 4000 m depth in both the eastern and western sides of the basin.

4. Results

Lead concentrations and isotope compositions of all South Atlantic samples are provided in Tables 1 and 2 and are shown in Fig. 3. Lead concentrations vary between 4.9 ± 0.4 pmol/kg (GA10 Station 18, 3983 m) and 36.3 ± 0.6 pmol/kg (GA02 Station 7, 5033 m) and generally, decrease from surface to bottom waters (Fig. 3). The only exceptions are two samples from GA02 (Station 7, 5033 m, and Station 3, 5715 m), where concentrations above 35 pmol/kg are observed at the deepest depth, in correspondence to a thick nepheloid layer, as evidenced by the reduced beam transmittance values recorded at the time of sampling (Fig. S4). The decrease in Pb concentrations from surface to depth is visible when grouping samples based on water masses (Fig. 4), with the mixed layer showing the largest median value, and NADW and AABW the lowest. Considering mean rather than median values, AABW shows a higher concentration (13.1 ± 12.2 pmol/kg, n = 11, 1SD) than the two water masses above it, namely NADW (11.3 ± 4.5 pmol/kg, n = 24, 1SD) and UCDW (12.9 ± 1.4 pmol/kg, n = 4, 1SD), due to the high concentrations recorded for the near-bottom samples collected at GA02 Stations 3 and 7, although they all remain identical within error. Two vertically adjacent water masses, SACW ([Pb] = 17.5 ± 2.3 pmol/kg, n = 19, 1SD) and AAIW ([Pb] = 13.2 ± 1.8 pmol/kg, n = 14, 1SD), have statistically different Pb concentrations (p-value < 0.05; Table S4).

Lead isotope ratios vary between 1.1431 and 1.1943 for $^{206}Pb/^{207}Pb$, and 2.4153 and 2.4727 for $^{208}Pb/^{207}Pb$. All depth profiles show a general progressive decreasing trend in $^{206}Pb/^{207}Pb$ and $^{208}Pb/^{207}Pb$ between 0 and 1000 m, with minima coinciding with the core of Antarctic Intermediate Water (Fig. 3). Lead isotope ratios then display an overall increase towards higher values at depth. Interestingly, the two deepest samples collected at Station 12 (GA10) show distinct Pb isotope compositions and concentrations even though they were collected only 44 m apart in the water column. This difference is attributed to the likely presence of hydrothermal activity at the Mid-Atlantic Ridge at that location (Rüth et al., 2000; Saito et al., 2013).

Water masses also reveal statistically significant differences in their Pb isotope compositions (Tables S5, S6). The mixed layer and SACW have significantly different Pb isotope compositions based on $^{206}Pb/^{207}Pb$ (p-value < 0.05; Table S6). Additionally, the Pb isotope composition of AABW ($^{206}Pb/^{207}Pb$ = 1.1847 ± 0.0152; $^{208}Pb/^{207}Pb$ = 2.4613 ± 0.0173; n = 11, 2SD) is statistically distinct from all other intermediate and deep water masses ventilating in the Southern Hemisphere, namely SACW ($^{206}Pb/^{207}Pb$ = 1.1588 ± 0.0098; $^{208}Pb/^{207}Pb$ = 2.4314 ± 0.0091; n = 19, 2SD), AAIW ($^{206}Pb/^{207}Pb$ = 1.1562 ± 0.0061; $^{208}Pb/^{207}Pb$ = 2.4300 ± 0.0073; n = 14, 2SD), and UCDW ($^{206}Pb/^{207}Pb$ = 1.1618 ± 0.0102; $^{208}Pb/^{207}Pb$ = 2.4366 ± 0.0094; n = 4, 2SD). Due to its large variability, the Pb isotope composition of NADW ($^{206}Pb/^{207}Pb$ = 1.1726 ± 0.0152; $^{208}Pb/^{207}Pb$ = 2.4455 ± 0.0146; n = 24, 2SD) is identical within uncertainty to that of UCDW and AABW, the water masses located directly above and below.

5. Discussion

5.1. Remobilisation of previously deposited PB

Near-bottom samples collected at GA02 Stations 3 (5715 m) and 7 (5033 m) show the highest Pb concentrations (36–36.3 pmol/kg) and isotope compositions ($^{206}Pb/^{207}Pb$ = 1.194; $^{208}Pb/^{207}Pb$ = 2.472–2.473) of the whole dataset and were sampled in a thick nepheloid layer (Fig. 3, Fig. S4). The remobilisation of material at depth, inferred by the reduced transmittance values at the sampling locations, is also supported by the observation of black fibres in both two 1 L HDPE bottles containing the sample from Station 3 (GA02). Previously published data on DPb concentrations for these two sampling locations are between 4 and 5 pmol/kg, indicating that the particulate phase contributed most of the Pb measured in the unfiltered samples (Fig. S1; GEOTRACES Intermediate Data Product Group, 2021). This evidence suggests that the different Pb isotope compositions observed for the two samples from Stations 3 and 7 compared to the rest of the AABW samples ($^{206}Pb/^{207}Pb$ = 1.1826 ± 0.0134; $^{208}Pb/^{207}Pb$ = 2.4589 ± 0.0150) are caused by Pb release from suspended particles.

The Pb isotope compositions of these two nepheloid layer samples are in agreement with the surface layer data of two Fe-Mn crusts from the western South Atlantic ($^{206}Pb/^{207}Pb$ = 1.194–1.204; $^{208}Pb/^{207}Pb$ = 2.474–2.485; von Blanckenburg et al., 1996), supporting a natural origin of the Pb present in the near-bottom layer. This indicates that anthropogenic Pb inputs, with lower $^{206}Pb/^{207}Pb$ and $^{208}Pb/^{207}Pb$ values than natural Pb sources (Fig. S5), have not significantly impacted

Table 1
Pb concentrations and isotope compositions as well as sampling information for GEOTRACES cruise GA02 Leg 3 water samples analysed in this study. Salinity and temperature data obtained from the GEOTRACES Intermediate Data Product Group (2021).

Sample		Water properties			Pb concentration			Pb isotope composition												
ID	Depth (m)	Temperature (°C)	Salinity	Water Mass*	[Pb] ± 1 SD[a] (pmol/kg)			$^{206}Pb/^{207}Pb$ ± 2 SD[b]			$^{208}Pb/^{207}Pb$ ± 2 SD[b]			$^{206}Pb/^{204}Pb$ ± 2 SD[b]			$^{207}Pb/^{204}Pb$ ± 2 SD[b]			$^{208}Pb/^{204}Pb$ ± 2 SD[b]		
Station 3 (-46.92 °N, -47.21 °E) - 08/03/2011																				
24[c]	10	17.04	34.62	MIX	10.1	±	0.2	1.17228	±	4	2.44303	±	8	18.3307	±	38	15.6369	±	35	38.201	±	9
22	49	14.26	35.07	MIX	28.7	±	1.4	1.16522	±	3	2.43628	±	6	18.2004	±	16	15.6195	±	15	38.053	±	4
18	200	10.47	34.85	MIX	14.6	±	1.0	1.16596	±	4	2.43808	±	12	18.2250	±	31	15.6308	±	30	38.110	±	9
14	502	4.23	34.13	AAIW	13.2	±	0.8	1.15515	±	4	2.42855	±	9	18.0292	±	25	15.6084	±	22	37.907	±	6
13	751	3.49	34.21	AAIW	15.8	±	0.0	1.15590	±	3	2.42924	±	8	18.0373	±	18	15.6044	±	18	37.907	±	5
12	1002	2.98	34.31	AAIW	11.9	±	0.6	1.15661	±	3	2.43035	±	10	18.0438	±	26	15.6000	±	25	37.916	±	6
10	1501	2.75	34.57	UCDW	12.2	±	1.5	1.16052	±	4	2.43610	±	8	18.1217	±	29	15.6146	±	28	38.041	±	7
7	3001	1.97	34.77	NADW	7.6	±	0.7	1.17652	±	4	2.45077	±	8	18.3908	±	27	15.6315	±	24	38.307	±	6
5	4001	0.90	34.71	AABW	6.1	±	0.7	1.18394	±	4	2.46010	±	7	18.5345	±	31	15.6547	±	25	38.513	±	7
3	5001	0.37	34.67	AABW	6.9	±	2.0	1.18272	±	6	2.46131	±	11	18.5176	±	44	15.6574	±	33	38.537	±	9
1	5715	0.34	34.67	AABW	36.0	±	0.3	1.19434	±	2	2.47218	±	6	18.6821	±	17	15.6419	±	14	38.669	±	4
Station 7 (-37.84 °N, -41.13 °E) - 12/03/2011																				
24	10	20.42	35.41	MIX	16.6	±	0.3	1.17508	±	3	2.44425	±	6	18.3873	±	16	15.6476	±	17	38.247	±	4
22	49	19.54	35.52	MIX	18.5	±	1.1	1.17041	±	2	2.44105	±	7	18.3045	±	21	15.6393	±	19	38.177	±	5
18	200	14.72	35.58	SACW	14.7	±	0.3	1.16265	±	3	2.43477	±	7	18.1494	±	18	15.6098	±	18	38.007	±	5
14	500	8.85	34.62	SACW	14.1	±	0.2	1.16114	±	3	2.43358	±	7	18.1378	±	21	15.6206	±	20	38.015	±	6
12	1002	3.67	34.24	AAIW	15.3	±	1.1	1.15566	±	5	2.42958	±	10	18.0283	±	28	15.5998	±	26	37.902	±	7
10	1501	2.89	34.50	UCDW	14.6	±	0.4	1.15848	±	3	2.43414	±	7	18.0831	±	25	15.6089	±	25	37.996	±	7
7	2500	2.60	34.82	NADW	12.1	±	0.1	1.17649	±	3	2.44917	±	9	18.3814	±	27	15.6233	±	25	38.266	±	7
5	3499	1.24	34.73	NADW	6.0	±	1.7	1.17666	±	4	2.45362	±	9	18.3926	±	33	15.6309	±	29	38.352	±	7
3	4502	0.31	34.67	AABW	7.0	±	0.8	1.18596	±	5	2.46382	±	7	18.5479	±	34	15.6407	±	30	38.534	±	7
1	5033	0.26	34.67	AABW	36.3	±	0.6	1.19402	±	3	2.47270	±	7	18.6799	±	19	15.6444	±	18	38.683	±	5
Station 11 (-26.09 °N, -34.28 °E) - 17/03/2011																				
24	10	25.91	36.53	MIX	23.0	±	1.2	1.16948	±	2	2.43735	±	5	18.2897	±	15	15.6391	±	15	38.117	±	4
22	52	22.88	36.73	MIX	20.3	±	0.3	1.16513	±	2	2.43480	±	6	18.2069	±	18	15.6265	±	16	38.048	±	5
18	201	17.35	35.85	SACW	20.0	±	0.0	1.15854	±	2	2.43072	±	6	18.0956	±	17	15.6192	±	15	37.965	±	4
14	502	10.63	34.88	SACW	17.6	±	0.1	1.15594	±	2	2.42957	±	7	18.0556	±	18	15.6197	±	17	37.950	±	5
13	750	5.73	34.38	AAIW	15.2	±	0.0	1.15625	±	3	2.42872	±	6	18.0430	±	17	15.6045	±	15	37.899	±	4
12	997	3.82	34.38	AAIW	15.8	±	2.4	1.15910	±	3	2.43299	±	6	18.0954	±	21	15.6114	±	19	37.983	±	5
10	1499	3.28	34.75	UCDW	13.3	±	0.9	1.16935	±	4	2.44338	±	8	18.2700	±	29	15.6234	±	26	38.175	±	7
7	2502	3.01	34.93	NADW	18.4	±	1.2	1.18308	±	2	2.45451	±	6	18.5010	±	18	15.6379	±	17	38.383	±	5
5	3001	2.73	34.92	NADW	12.4	±	0.0	1.18362	±	4	2.45448	±	9	18.5077	±	29	15.6361	±	27	38.380	±	7
3	3500	2.32	34.88	NADW	11.9	±	0.8	1.18319	±	4	2.45582	±	9	18.5006	±	32	15.6358	±	29	38.398	±	8
1	4560	0.29	34.67	AABW	8.8	±	1.0	1.18779	±	4	2.46410	±	10	18.5864	±	31	15.6487	±	29	38.558	±	8
Station 16 (-5.68 °N, -28.46 °E) - 24/03/2011																				
24[c]	**10**	28.88	36.28	MIX	19.0	±	0.6	1.17078	±	6	2.44559	±	11	18.3100	±	33	15.6398	±	28	38.247	±	8
22	49	28.66	36.45	MIX	16.6	±	0.2	1.16581	±	3	2.44324	±	8	18.2426	±	26	15.6478	±	24	38.232	±	7
21	73	27.80	36.72	MIX	18.2	±	0.8	1.16597	±	2	2.44141	±	7	18.2247	±	16	15.6302	±	14	38.160	±	4
19	149	16.23	35.72	SACW	19.4	±	2.8	1.15846	±	3	2.43409	±	9	18.1037	±	24	15.6275	±	21	38.039	±	6
18	199	11.36	35.09	SACW	20.2	±	2.3	1.15805	±	3	2.43173	±	7	18.0864	±	18	15.6179	±	17	37.978	±	5
12	1000	4.17	34.56	AAIW	10.8	±	0.7	1.16533	±	4	2.44107	±	11	18.2206	±	28	15.6348	±	26	38.167	±	7
10	1500	4.21	34.95	NADW	20.7	±	0.2	1.17968	±	3	2.44914	±	5	18.4334	±	13	15.6255	±	12	38.269	±	3
7	2500	2.88	34.92	NADW	9.9	±	0.1	1.18196	±	5	2.45471	±	10	18.4887	±	41	15.6421	±	39	38.397	±	11
5	3501	2.52	34.91	NADW	16.9	±	0.3	1.18340	±	3	2.45418	±	8	18.5029	±	21	15.6352	±	20	38.372	±	6
1	5532	0.72	34.70	AABW	9.4	±	0.3	1.18835	±	4	2.46320	±	13	18.6131	±	36	15.6640	±	33	38.580	±	9

* Water mass attribution performed as part of the study using temperature and salinity data.
[a] The uncertainties of the concentration data represent 1SD of the duplicate concentration analyses conducted for each sample.
[b] Uncertainty refers to the last digit(s) of the mean value.
[c] Sample previously published in Olivelli et al. (2023).

Table 2
Pb concentrations and isotope compositions as well as sampling information for GEOTRACES cruise GA10 water samples analysed in this study. Salinity and temperature data obtained from the GEOTRACES Intermediate Data Product Group (2021). Data for Station 3 were previously published in Paul et al. (2015a).

Sample		Water properties			Pb concentration			Pb isotope composition												
ID	Depth (m)	Temperature (°C)	Salinity	Water Mass*	[Pb] ± 1 SD[a] (pmol/kg)			$^{206}Pb/^{207}Pb$ ± 2 SD[b]			$^{208}Pb/^{207}Pb$ ± 2 SD[b]			$^{206}Pb/^{204}Pb$ ± 2 SD[b]			$^{207}Pb/^{204}Pb$ ± 2 SD[b]			$^{208}Pb/^{204}Pb$ ± 2 SD[b]		
Station 3[c] (-36.47 °N, 13.26 °E) - 23/10/2010																				
21	25	12.08	34.88	MIX	20.5	±	0.4	1.15920	±	3	2.43330	±	6	18.1110	±	18	15.6240	±	16	38.017	±	4
18	49	12.05	34.88	MIX	25.2	±	0.5	1.15332	±	4	2.42814	±	9	18.0130	±	19	15.6180	±	18	37.922	±	5
15	99	11.17	34.74	MIX	22.4	±	0.8	1.15563	±	4	2.42993	±	8	18.0440	±	18	15.6140	±	16	37.941	±	4
12	198	10.70	34.76	SACW	17.3	±	0.6	1.15980	±	5	2.43271	±	8	18.1250	±	27	15.6270	±	24	38.015	±	6
9	397	8.15	34.55	SACW	21.2	±	0.6	1.15808	±	5	2.43126	±	9	18.0870	±	35	15.6180	±	30	37.970	±	8
8	594	5.22	34.29	SACW	15.7	±	0.5	1.15582	±	7	2.42853	±	9	18.0310	±	25	15.6000	±	22	37.885	±	5
7	989	3.64	34.41	AAIW	11.5	±	0.5	1.15400	±	5	2.42941	±	9	18.0070	±	26	15.6040	±	24	37.911	±	6
5	1975	2.68	34.81	NADW	9.6	±	0.4	1.16718	±	6	2.44250	±	13	18.2340	±	46	15.6230	±	40	38.159	±	10
4	2955	2.29	34.84	NADW	5.3	±	0.4	1.17191	±	9	2.44688	±	22	18.4180	±	84	15.7170	±	73	38.452	±	18
2	3931	1.27	34.75	NADW	6.1	±	0.4	1.17578	±	8	2.44914	±	16	18.3700	±	63	15.6250	±	53	38.266	±	13
1	4724	1.10	34.73	AABW	7.1	±	0.4	1.18354	±	7	2.46021	±	16	18.5400	±	57	15.6640	±	51	38.537	±	13
Station 6 (-40.01 °N, 0.87 °E) -29/10/2010																				
21	25	10.61	34.54	MIX	19.9	±	0.4	1.16383	±	4	2.43310	±	8	18.1889	±	26	15.6290	±	23	38.028	±	5
18	49	10.45	34.54	MIX	26.5	±	1.4	1.16160	±	5	2.43378	±	13	18.1400	±	30	15.6165	±	26	38.006	±	7
15	100	10.10	34.54	MIX	25.5	±	0.4	1.16165	±	3	2.43363	±	5	18.1549	±	15	15.6277	±	14	38.033	±	3
12	200	9.51	34.65	SACW	19.8	±	0.4	1.16310	±	4	2.43459	±	6	18.1749	±	19	15.6261	±	16	38.043	±	4
9	401	6.40	34.36	SACW	17.3	±	0.4	1.15908	±	4	2.43125	±	6	18.1088	±	21	15.6249	±	19	37.987	±	5
8	600	4.60	34.23	SACW	17.3	±	0.4	1.15683	±	3	2.42928	±	7	18.0560	±	17	15.6087	±	16	37.918	±	4
7	999	3.22	34.33	AAIW	12.9	±	0.4	1.15571	±	3	2.42876	±	5	18.0239	±	15	15.5954	±	13	37.878	±	3
5	1999	2.65	34.77	NADW	8.0	±	0.4	1.16863	±	5	2.44168	±	8	18.2534	±	32	15.6186	±	28	38.135	±	7
4	2998	2.20	34.83	NADW	7.1	±	0.4	1.16751	±	7	2.44102	±	12	18.2333	±	38	15.6167	±	34	38.121	±	9
2	4000	1.26	34.75	NADW	6.0	±	0.4	1.17338	±	10	2.44624	±	16	18.3183	±	51	15.6119	±	44	38.189	±	11
1	4500	1.11	34.73	AABW	8.5	±	0.4	1.18098	±	11	2.45551	±	24	18.4384	±	76	15.6187	±	66	38.350	±	16
Station 8_r (-34.31 °N, 17.59 °E) - 19/11/2010																				
21	25	17.75	35.49	SHELF	31.9	±	0.4	1.16022	±	5	2.45007	±	9	18.1469	±	22	15.6423	±	19	38.324	±	5
17	51	17.52	35.49	SHELF	28.4	±	0.4	1.16016	±	3	2.44969	±	5	18.1477	±	15	15.6419	±	13	38.318	±	3
13	100	14.24	35.26	SHELF	21.7	±	0.4	1.15415	±	4	2.43459	±	8	18.0296	±	16	15.6220	±	15	38.034	±	4
9	199	12.38	35.06	SHELF	23.1	±	0.4	1.15397	±	10	2.43110	±	21	18.0379	±	45	15.6318	±	41	38.001	±	11
5	401	8.48	34.64	SHELF	25.1	±	0.4	1.16776	±	4	2.44346	±	6	18.2601	±	18	15.6367	±	16	38.208	±	4
1	719	5.54	34.41	SHELF	16.1	±	0.4	1.15920	±	4	2.43485	±	8	18.1049	±	29	15.6188	±	25	38.030	±	6
Station 12 (-40.00 °N, -16.47 °E) - 10/01/2012																				
	16	16.31	35.17	MIX	20.3	±	0.5	1.16164	±	5	2.43255	±	10	18.1402	±	23	15.6160	±	21	37.986	±	5
	42	16.27	35.17	MIX	17.3	±	0.5	1.16369	±	3	2.43446	±	6	18.1942	±	20	15.6343	±	18	38.062	±	4
	95	12.94	35.26	MIX	16.4	±	0.4	1.16697	±	3	2.43781	±	6	18.2431	±	16	15.6331	±	14	38.109	±	4
	193	12.41	35.21	SACW				1.16531	±	5	2.43556	±	9	18.2026	±	28	15.6206	±	25	38.045	±	6
	492	8.27	34.57	SACW	15.7	±	0.4	1.16076	±	3	2.43249	±	7	18.1277	±	17	15.6167	±	16	37.987	±	4
	990	3.58	34.26	AAIW	14.0	±	0.4	1.15444	±	3	2.42719	±	5	18.0099	±	16	15.6011	±	14	37.867	±	4
	1488	2.85	34.50	UCDW	11.5	±	0.5	1.15889	±	7	2.43280	±	16	18.0688	±	48	15.5918	±	42	37.929	±	11
	1987	2.81	34.75	NADW	13.7	±	0.4	1.16500	±	10	2.43800	±	18	18.1701	±	80	15.5969	±	70	38.022	±	17
	2487	2.62	34.82	NADW	16.4	±	0.4	1.16671	±	8	2.43851	±	10	18.1767	±	49	15.5820	±	45	37.991	±	11
	2988	2.13	34.83	NADW	10.0	±	0.4	1.16577	±	6	2.43903	±	11	18.2027	±	37	15.6142	±	32	38.084	±	8
	3031	2.12	34.82	NADW	7.7	±	0.4	1.17604	±	7	2.44820	±	11	18.3448	±	44	15.5967	±	39	38.188	±	10
Station 18 (-40.00 °N, -42.42 °E) - 19/01/2012																				
	45	13.13	35.04	MIX	16.7	±	0.4	1.16884	±	4	2.44104	±	11	18.2551	±	22	15.6176	±	19	38.124	±	5
	96	11.34	34.94	MIX				1.16207	±	3	2.43380	±	6	18.1365	±	16	15.6080	±	13	37.987	±	3
	197	7.49	34.39	SACW	14.4	±	0.4	1.16109	±	5	2.43413	±	8	18.1193	±	21	15.6061	±	20	37.988	±	5
	494	4.40	34.18	SACW	15.0	±	0.4	1.15403	±	4	2.42731	±	7	18.0128	±	17	15.6080	±	16	37.885	±	4
	742	3.49	34.23	AAIW	12.5	±	0.4	1.15227	±	4	2.42564	±	7	17.9634	±	26	15.5902	±	24	37.815	±	6
	992	3.03	34.37	AAIW	12.5	±	0.4	1.15536	±	4	2.42942	±	8	18.0296	±	22	15.6046	±	20	37.912	±	5

(*continued on next page*)

Table 2 (*continued*)

Sample		Water properties			Pb concentration				Pb isotope composition								
ID	Depth (m)	Temperature (°C)	Salinity	Water Mass*	[Pb] ± 1 SD[a] (pmol/kg)				$^{206}Pb/^{207}Pb \pm 2$ SD[b]				$^{208}Pb/^{207}Pb \pm 2$ SD[b]				$^{206}Pb/^{204}Pb \pm 2$ SD[b]				$^{207}Pb/^{204}Pb \pm 2$ SD[b]				$^{208}Pb/^{204}Pb \pm 2$ SD[b]			
	1990	2.91	34.81	NADW	15.8	±	0.8		1.16543	±	7		2.43753	±	12		18.2180	±	55		15.6327	±	46		38.107	±	12	
	2488	2.56	34.84	NADW	14.2	±	0.4		1.15727	±	3		2.42963	±	6		18.0442	±	16		15.5923	±	14		37.885	±	3	
	2988	1.70	34.76	NADW					1.16475	±	6		2.43819	±	13		18.1545	±	34		15.5866	±	31		38.004	±	8	
	3983	0.55	34.69	AABW	4.9	±	0.4		1.16581	±	6		2.44014	±	9		18.1990	±	32		15.6111	±	29		38.093	±	7	
	5103	0.25	34.67	AABW					1.18417	±	5		2.46151	±	8		18.4970	±	26		15.6218	±	23		38.453	±	6	
Station 21 (-37.02 °N, -52.50 °E) -24/01/2012																												
	56	21.90	36.72	MIX					1.16651	±	4		2.43655	±	7		18.2438	±	24		15.6411	±	21		38.109	±	5	
	88	20.53	36.52	MIX	20.0	±	0.6		1.16390	±	4		2.43320	±	5		18.2022	±	15		15.6389	±	13		38.052	±	3	
	197	16.28	35.79	SACW	19.6	±	1.5		1.16604	±	4		2.43597	±	6		18.2185	±	14		15.6241	±	12		38.061	±	3	
	296	14.79	35.55	SACW					1.14309	±	4		2.41527	±	8		18.1097	±	12		15.5898	±	12		37.653	±	3	
	510	10.38	34.86	SACW	17.9	±	0.5		1.15916	±	4		2.43275	±	5		17.8204	±	21		15.6232	±	19		38.008	±	5	
	992	3.61	34.22	AAIW	11.7	±	0.4		1.15473	±	10		2.42828	±	23		18.0252	±	33		15.6099	±	30		37.905	±	8	
	1492	3.50	34.47	AAIW	10.9	±	0.5		1.15655	±	4		2.43164	±	8		18.0552	±	21		15.6103	±	18		37.960	±	5	
	1993	2.87	34.80	NADW	15.4	±	0.4		1.16322	±	6		2.43609	±	11		18.1590	±	31		15.6098	±	29		38.027	±	7	
	2987	1.35	34.75	NADW	9.7	±	0.4		1.16891	±	6		2.44281	±	10		18.2498	±	33		15.6123	±	29		38.136	±	7	
	3355				6.6	±	0.4		1.17404	±	7		2.44898	±	12		18.3455	±	36		15.6267	±	31		38.270	±	8	

* Water mass attribution performed as part of the study using temperature and salinity data.
[a] The uncertainties of the concentration data propagate both the (within-run) precision of the isotopic analyses and the uncertainty of the blank correction.
[b] Uncertainty refers to the last digit(s) of the mean value.
[b] Depth profile previously published in Paul et al. (2015a).

the bottom sediments of the geographically remote area of the Argentine Basin. By contrast, Pb isotope compositions of AABW collected outside of the nepheloid layer feature lower Pb isotope ratios than the Fe-Mn crusts. This suggests that anthropogenic Pb pollution has reached AABW, possibly due to sinking of polluted surface waters around Antarctica (Bertinetti et al., 2020; Planchon et al., 2003). Nevertheless, AABW remains the water mass with the most natural Pb isotope composition of the South Atlantic Ocean ($^{206}Pb/^{207}Pb = 1.1826 \pm 0.0134$; $^{208}Pb/^{207}Pb = 2.4589 \pm 0.0150$).

In the context of previously published literature data, high concentrations of DPb together with an isotopic composition of $^{206}Pb/^{207}Pb \sim 1.180$ at near-bottom depths were reported for a nepheloid layer in the Western Philippines Sea, at locations much closer to land than GA02 Stations 3 and 7 (Chien et al., 2017). In the Western Philippines Sea, the DPb isotope compositions of seawater samples differed from Fe-Mn crust deposits but was influenced by sedimentary inputs from the shelf. In this case, the sediments did not carry an entirely natural signature, as their Pb isotope compositions had less natural values than those of Fe-Mn crusts. Other studies observed either low concentrations of DPb with a predominantly natural Pb isotope composition due to boundary exchange at the sediment-water interface (Okinawa Trough; Chen et al., 2023) or high concentrations of DPb with a predominantly anthropogenic Pb isotope signature in a thin nepheloid layer due to remobilisation of previously deposited Pb (North Atlantic Ocean; Noble et al., 2015). Therefore, to our knowledge, this is the first time that high concentrations of remobilised natural Pb were observed at near-bottom depth in the open ocean. However, caution must be exercised when comparing our TDPb observations with published DPb data, as the TDPb isotopic signature might be dominated by the remobilised particulates rather than the dissolved phase (SI, Note 1).

The Argentine Basin, where our samples were collected, is an area of high eddy kinetic energy. This contributes to the presence of a strong benthic nepheloid layer that has been observed since the 1960s, suggesting that the reduced beam transmittance recorded at the time of sampling is not an anomalous event (Gardner et al., 2018; Hernández-Molina et al., 2008). Therefore, the natural Pb isotope signatures of the two near-bottom samples at GA02 Stations 3 and 7 likely reflects a lack of deposition of modern sediments enriched in anthropogenic Pb, due high abyssal current velocities related to benthic storms (Richardson et al., 1993).

5.2. An eOMP perspective on Pb isotopes as tracers of large-scale ocean circulation

One interesting observation that can be made when comparing the distribution of Pb isotope compositions and conservative hydrographic parameters, such as salinity, is that they both seem to highlight the presence of isopycnal transport in the South Atlantic Ocean (Fig. 5). While this is especially true when looking at the intermediate water depths, corresponding to AAIW, the statistical differences in Pb isotope compositions observed between water masses (Table S5, S6) and their characteristic distribution, reflected in the shape of the water-mass-box plot of Fig. 4, provide evidence for isopycnal transport of the isotopic signature of Pb throughout most of the South Atlantic basin. Moreover, the Pb isotope composition of AAIW in the South Atlantic Ocean presented in this study is identical within error to that of the Indian Ocean ($^{206}Pb/^{207}Pb = 1.1489 \pm 0.0061$; $^{208}Pb/^{207}Pb = 2.4261 \pm 0.0095$; n = 6; Lee et al., 2015; Paul et al., 2015b). Furthermore, the Pb isotope signature of NADW in the two northernmost stations sampled here, Stations 11 and 16 of GA02, is well in agreement with that of the eastern tropical Atlantic ($^{206}Pb/^{207}Pb = 1.1762–1.1840$; $^{208}Pb/^{207}Pb = 2.4482–2.4545$; Bridgestock et al., 2018). These observations, together with the successful use of Pb isotopes as tracers of circulation patterns of northern-sourced water masses in the Atlantic Ocean (Alleman et al., 1999; Bridgestock et al., 2018; Véron et al., 1999), are indicative of isopycnal transport of Pb within and outside of the South Atlantic basin.

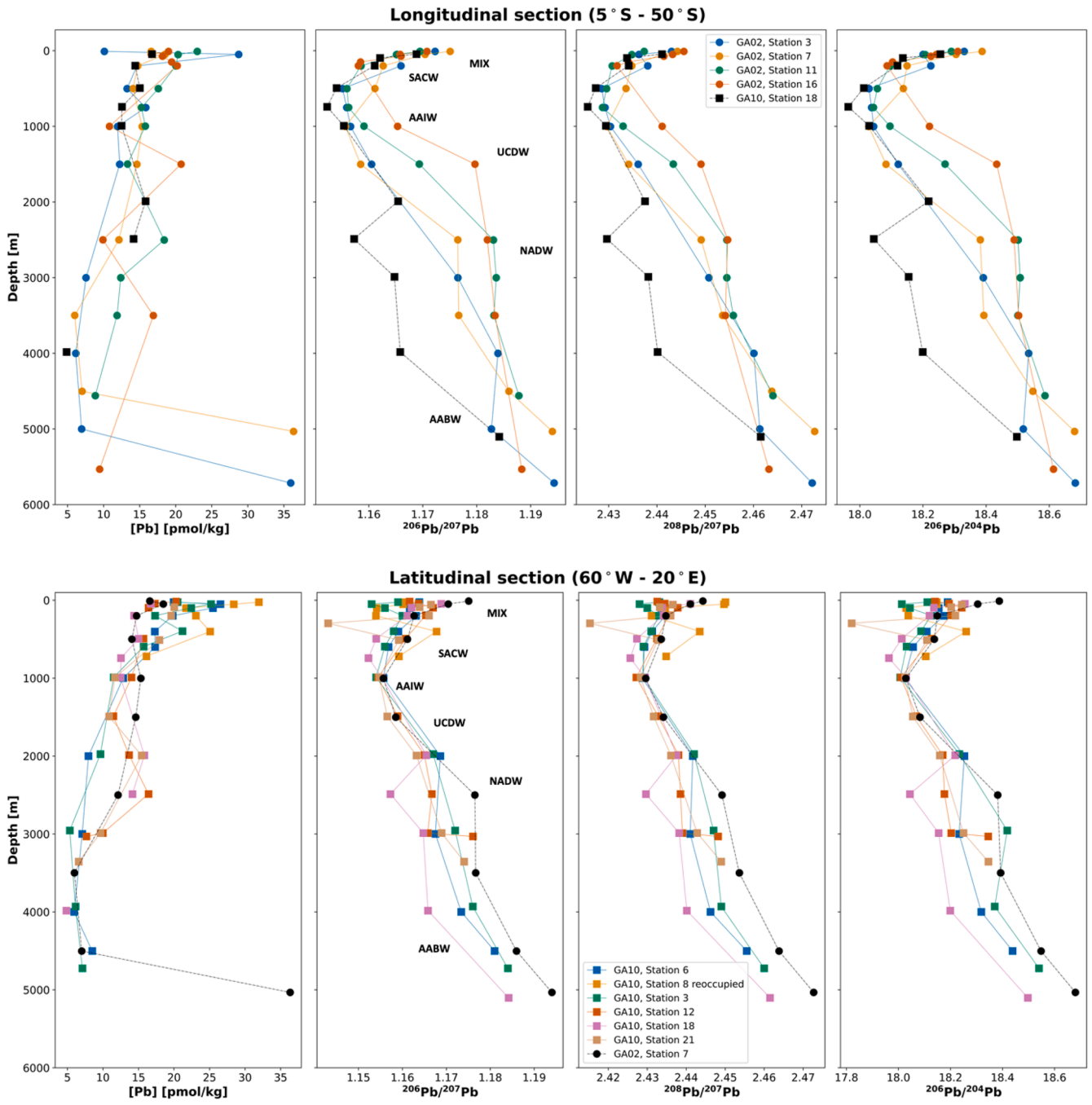

Fig. 3. Depth profiles of Pb concentrations, ^{206}Pb/^{207}Pb, ^{208}Pb/^{207}Pb and ^{206}Pb/^{204}Pb for the longitudinal (top) and latitudinal section (bottom). The longitudinal section includes all GA02 stations plus GA10 Station 18. The latitudinal section corresponds to the GA10 section, and its panel includes the data for GA02 Station 7 for reference. Error bars for Pb isotope ratios are smaller than the symbols; Pb concentration errors are available in Tables 1 and 2. Water masses labels are the same as in Fig. 2.

To constrain the extent of the isopycnal transport of Pb, an extended optimum multiparameter (eOMP) analysis was conducted using the new Pb results of this study together with hydrographic data from GEOTRACES cruises GA02 and GA10. The model set up for the eOMP analysis builds upon previous efforts to constrain the cycling of Cd, Ni and Zn along the entire GEOTRACES GA02 section (Middag et al., 2018, 2019, 2020). The eOMP methodology, firstly developed by Tomczak (1981), is used to quantify the contributions of pre-defined endmember water masses to each water sample collected and analysed as part of this study, based on five tracers (potential temperature, salinity, NO_3^-, Si, O_2; see Table S1 in Middag et al., 2018), and the effects of remineralisation. A more in-depth explanation is provided in the Supplementary Information (Note 2). All five water masses observed (SACW, AAIW, UCDW, NADW, and AABW) are included in the eOMP analysis to model the isopycnal transport of Pb concentrations and isotope compositions. Each water mass is assigned endmember values for Pb concentration and ^{206}Pb/^{207}Pb, ^{208}Pb/^{207}Pb ratios, corresponding to the values observed at the 'position of entry into the study region', and a 95 % confidence interval that is used to assess the uncertainty of the modelled results using a Monte Carlo analysis (Table S7 and SI Note 2). The assigned values are hence those observed at the northernmost location (GA02 Station 16) for NADW and at the southernmost location of the GA02 transect for all other water masses (SACW: Station 7; otherwise: Station 3). The two samples collected in the nepheloid layer are excluded from the eOMP

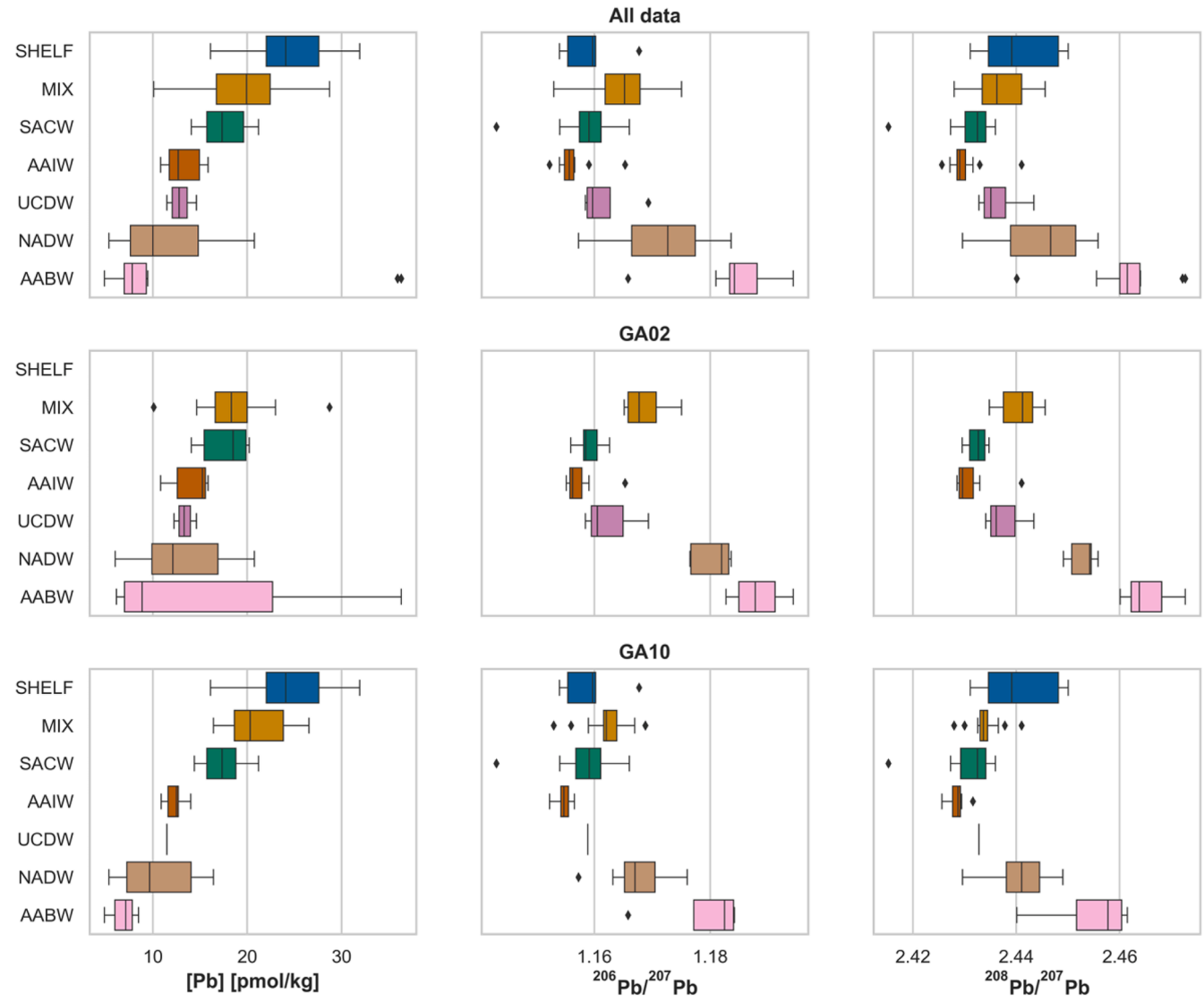

Fig. 4. Boxplots of Pb concentrations, $^{206}Pb/^{207}Pb$ and $^{208}Pb/^{207}Pb$ for the different water masses identified in the dataset. The top row includes all data (GA02 and GA10), while the middle and the bottom rows only include data for the GA02 and GA10 sections, respectively. Water masses labels are the same as in Fig. 2.

analysis as their Pb concentrations and isotope compositions are impacted by a localised process of sediment resuspension.

The differences observed between the modelled and observed distributions of Pb isotope compositions are reported in Fig. 6 and Table 3. Overall, the model is better at reproducing observations along the GA02 than the GA10 section, likely due to the use of GA02 data when defining the Pb endmembers to capture the predominantly meridional direction of water mass transport. In particular, the discrepancy between modelled results and observations is larger than the model's uncertainty for the vast majority of intermediate and deep water samples collected south of 40°S on GA02 and more broadly on GA10, where the offset between observed and modelled data is up to 40 times larger than for GA02 (Fig. 6). When observations fall outside a model's uncertainty interval, this indicates that the model does not fully reproduce the observed data. In the case of the eOMP analysis, this suggests that seawater Pb isotope compositions in the South Atlantic Ocean are consistent with isopycnal transport and mixing until around 40°S, where observed and modelled ratios are within uncertainty, but other processes must play a role at the Brazil-Malvinas Confluence and along the 40°S transect, where observed Pb isotope ratios fall outside the uncertainty interval of the model.

In detail, SACW and AABW, the top and bottom water masses considered, show the smallest discrepancies between modelled and observed data (Table 3). On the other hand, AAIW, UCDW, and NADW show the largest model-data offsets, particularly on GA10. Observations for NADW, which has travelled from high latitudes of the Northern Hemisphere to reach the South Atlantic, show that it has the most variable Pb isotope composition when considering the entire domain (Fig. 4, top row). This variability is reflected in the large discrepancies between observed and modelled $^{206}Pb/^{207}Pb$ and $^{208}Pb/^{207}Pb$ values of GA10 samples collected at depths corresponding to NADW, which is the water mass worst reconstructed by the eOMP model. As the NADW Pb endmember reflects the characteristics of the equatorial South Atlantic, the small offset between modelled and observed GA02 data, combined with the model's inability to reproduce GA10 samples, hints at the presence of a local phenomenon that affects the distribution of Pb isotope signatures at depths between 2000 and 4000 m along the 40°S section (Fig. 6). Additionally, the model is better at reproducing samples belonging to AAIW and UCDW, the two water masses located above NADW, along the GA02 section than along GA10. This further supports the hypothesis that a local phenomenon might affect Pb isotope compositions at 40°S.

Transient changes in the Pb concentration and isotope composition of NADW could be hypothesised to cause discrepancies between

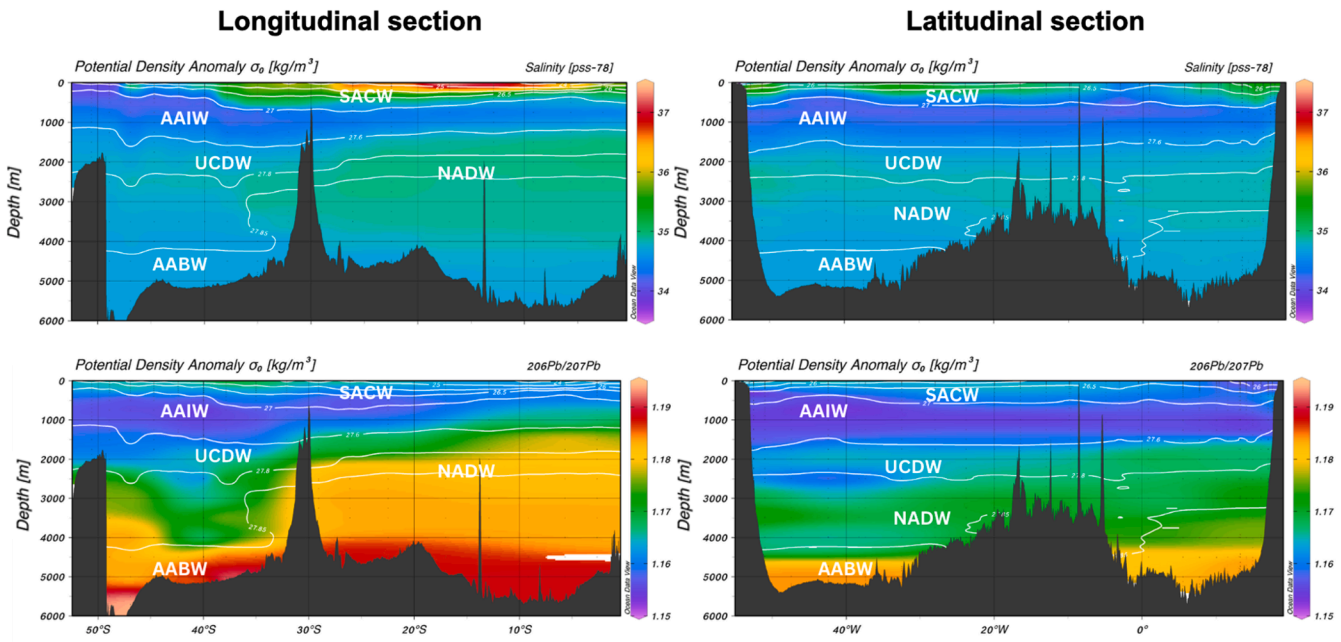

Fig. 5. Salinity (top) and $^{206}Pb/^{207}Pb$ (bottom) for the longitudinal and the latitudinal sections. The white contours represent the isopycnals identified by the potential density anomaly values reported on each line. Water masses labels are the same as in Fig. 2.

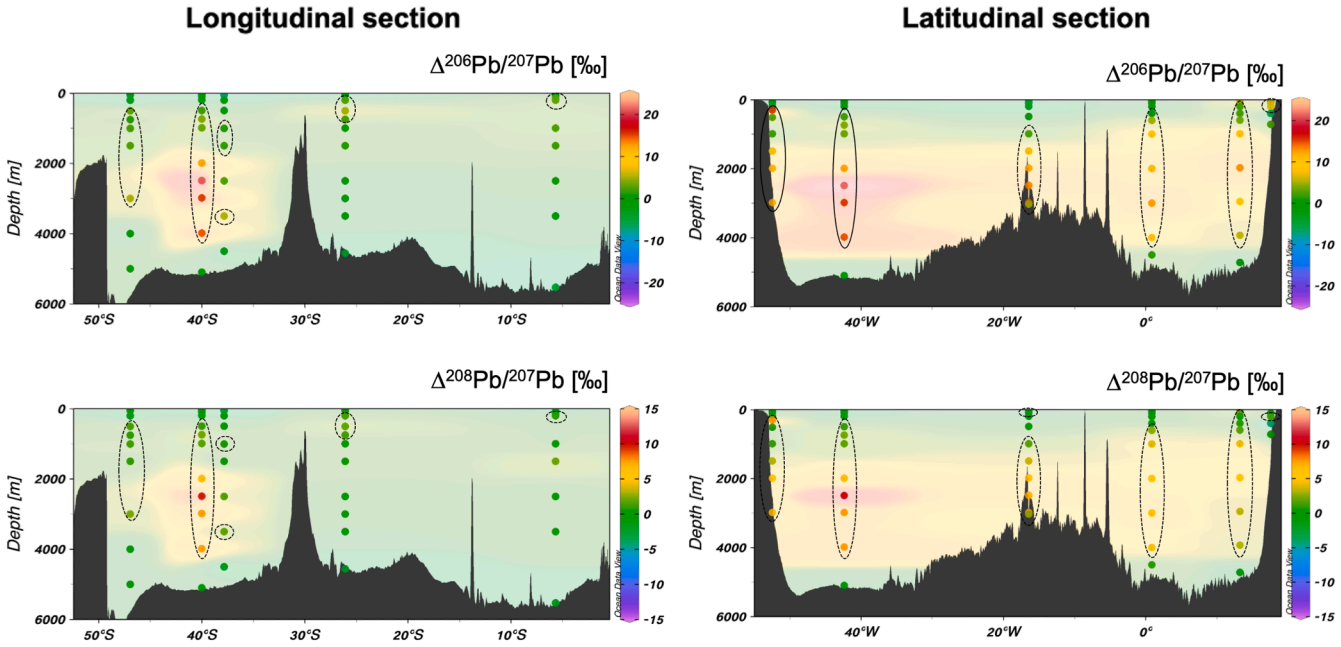

Fig. 6. Relative differences (as delta values in ‰) in modelled versus observed $^{206}Pb/^{207}Pb$ (top) and $^{208}Pb/^{207}Pb$ (bottom) ratios. Modelled values are obtained by the output of the eOMP analysis and do not include the two near-bottom samples for AABW collected in the nepheloid layer (Stations 3 and 7, GA02). Relative differences are calculated as $\Delta^{20x}Pb/^{207}Pb$ [‰] = [($^{20x}Pb/^{207}Pb$_model – $^{20x}Pb/^{207}Pb$_observation) / $^{20x}Pb/^{207}Pb$_observation]*1000. The shaded background represents an interpolation of the delta values for areas where observations were not available. Samples enclosed within black ellipses have a model-observation offset larger than the model's uncertainty.

observed and modelled values. However, if the difference was driven by a purely transient effect, the southernmost (older) waters along the GA02 section should be characterised by higher $^{206}Pb/^{207}Pb$ and $^{208}Pb/^{207}Pb$ values than the northernmost (younger) water, in agreement with the temporal evolution of the North Atlantic Pb isotope signature recorded in corals near Bermuda (Kelly et al., 2009). This is in contrast with the observations, which show that NADW samples collected at the more northern Stations 11 and 16 have higher Pb isotope ratios than those from the more southern Stations 3 and 7 (Fig. 3). Moreover, transient changes cannot explain the large differences in the Pb isotope compositions of the NADW samples from Station 7 (GA02) and Station 18 (GA10). These differences are unexpected as the stations are only separated by 265 km and they were sampled only 10 months apart.

Overall, this modelling exercise shows that Pb isotope ratios are good tracers of water mass movements for water masses that formed in the Atlantic sector of the Southern Ocean. However, deep water samples collected at latitudes higher than 35°S, and especially those from the

Table 3
Differences between modelled and observed distributions of Pb isotope compositions (206 Pb/207 Pb and 208 Pb/207 Pb) as a result of the eOMP analysis.

	$\Delta^{206}Pb/^{207}Pb$	$\Delta^{206}Pb/^{207}Pb$ [‰]	$\Delta^{208}Pb/^{207}Pb$	$\Delta^{208}Pb/^{207}Pb$ [‰]
		All data		
SACW (n = 19)	0.00208	*1.8*	0.00208	*0.9*
AAIW (n = 14)	0.00397	*3.4*	0.00391	*1.6*
UCDW (n = 4)	0.00325	*2.8*	0.00267	*1.1*
NADW (n = 21)	0.00896	*7.7*	0.00860	*3.5*
AABW (n = 9)	0.00028	*0.3*	-0.00006	*0.0*
		GA02		
SACW (n = 6)	0.00250	*2.2*	0.00159	*0.7*
AAIW (n = 7)	0.00191	*1.7*	0.00177	*0.7*
UCDW (n = 3)	0.00178	*1.5*	0.00093	*0.4*
NADW (n = 8)	0.00042	*0.4*	0.00029	*0.1*
AABW (n = 5)	-0.00274	*-2.3*	-0.00321	*-1.3*
		GA10		
SACW (n = 13)	0.00188	*1.6*	0.00230	*1.0*
AAIW (n = 7)	0.00603	*5.2*	0.00604	*2.5*
UCDW (n = 1)	0.00799	*6.9*	0.00786	*3.2*
NADW (n = 13)	0.01423	*12.2*	0.01366	*5.6*
AABW (n = 4)	0.00405	*3.5*	0.00388	*1.6*

GA10 section, differ significantly from the endmember compositions of the northernmost (NADW) and southernmost (AABW) samples. As NADW and AABW are the two endmembers that contribute the most to deep water samples collected at latitudes higher than 35°S, this difference causes a disagreement between observed and modelled values, with the former having more anthropogenic signatures than the latter. We here suggest that this discrepancy reflects that the advected Pb isotope ratios are altered by a local mechanism which transports pollution to depths of up to 4000 m (Fig. 6).

5.3. Evidence for vertical transport of anthropogenic Pb pollution at 40°S

The two near-crossover stations for GEOTRACES GA02 and GA10, Station 7 and Station 18, respectively (Fig. 1), have matching depth profiles in the top 2000 m but show discrepancies at greater depths (Fig. 3). These discrepancies are more evident in the Pb isotope compositions than the Pb concentrations, aside from the large Pb concentration spike in the nepheloid layer at Station 7 (Fig. 3). Hydrographic data collected at the two stations do not reveal any differences in terms of seawater properties (i.e. temperature, salinity, oxygen, and major nutrients; Fig. S6), demonstrating that the depth profiles sampled the same deep water masses.

The discrepancies in the Pb isotope data for the samples collected below 2000 m at the two stations may either reflect contamination or a natural origin. It is possible that some GA10 Station 18 samples were contaminated during sample handling, storage, or analysis either at sea or on land. This explanation is supported by the small 'kink' in the Station 18 profile data at ~2500 m, where a relatively high Pb concentration coincides with anomalously low Pb isotope ratios (Fig. 3). However, as the Pb concentrations observed at ~2500 m at Station 18 (14.2 ± 0.4 pmol/kg) and Station 7 (12.1 ± 0.1 pmol/kg) are not substantially different, there is no clear evidence that points towards a contamination event.

A natural origin of the observed discrepancy is therefore the preferred explanation. This conclusion is supported by the observation that other dissolved trace element concentrations (Al, Co, Ni) and DPb also show inconsistencies between the two profiles below 2000 m (GEOTRACES Intermediate Data Product Group, 2021; Fig. S7). In particular, Co and Ni concentrations show a 'kink' between 2000 and 3000 m in the Station 18 profile compared to that of Station 7, while Al concentrations between 2000 and 3000 m at Station 18 exceed those of Station 7 by up to a factor of two. Lastly, the depth profiles of DPb show an increase in concentrations between 2000 and 2500 m, with different values for the two stations. Overall, the collective evidence points towards an interesting natural anomaly between Station 18 (GA10) and Station 7 (GA02).

The recent study of Lanning et al. (2023) found that in areas of high surface productivity and high concentrations of suspended particulate matter (SPM) in the water column, the anthropogenic Pb isotope signature of surface waters can be transported to greater depths by reversible scavenging without significantly impacting the distribution of DPb concentrations. Furthermore, active scavenging in the surface and bottom 300 m of the water column was found in the vicinity of the East Pacific Rise by examining $^{210}Po/^{210}Pb$ profiles, while oligotrophic waters in the central tropical Pacific showed poor scavenging activity (Niedermiller and Baskaran, 2019; see also Planaj and Baskaran, 2024).

The Brazil – Malvinas Confluence, at 40°S, is an area of high productivity, as indicated by high surface chlorophyll-a concentrations (Garcia et al., 2004; Saraceno et al., 2005; Fig. 1B) and a high particulate organic matter flux from the euphotic zone to depth (Schlitzer et al., 2004). Additionally, high surface water chlorophyll-a concentrations are characteristic of the whole South Atlantic Subtropical Front (Mishonov et al., 2003; Thomalla et al., 2011), which coincides with the GA10 section (Fig. 1B). When analysing the distribution of $^{206}Pb/^{207}Pb$ and $^{208}Pb/^{207}Pb$ along the longitudinal section of this study, comprising all GA02 samples and Station 18 for GA10 (Fig. 7), the penetration of the anthropogenic Pb isotope signature to greater depths compared to the northern part of the section is visible between 2000 and 4000 m at 40°S in the western South Atlantic Ocean. When the depth profile of Station 18 (GA10) is excluded from the longitudinal section and the distribution of Pb isotope compositions is examined only for the cruise track of GA02 (Fig. 7), the penetration of anthropogenic Pb isotope signatures is still apparent but less visible. In particular, lower $^{206}Pb/^{207}Pb$ and $^{208}Pb/^{207}Pb$ values are still observed between 2000 and 3500 m in the Argentine basin (30–50°S) compared to the NADW signature observed between 0 and 30°S (Fig. 7). This evidence suggests that the discrepancies in the Pb isotope data between the profiles of Station 18 (GA10) and Station 7 (GA02) can be explained by the different extents to which the particle veil that is generated by SPM loads at ~40°S is expressed, reflecting distinct sampling locations and times of the year (January 2012 for Station 18, and March 2011 for Station 7). The profile observed at Station 18 (GA10) hence appears to reflect particularly strong reversible scavenging of Pb in the water column, facilitated by a higher SPM load at the time of sampling.

While vertical Pb transport is visible for NADW, other water masses above and below it, namely AAIW and AABW, should be affected by this mechanism as well. However, the highly anthropogenic background Pb isotope signature of AAIW will hinder the detection of vertical Pb transport at intermediate levels. Similarly, the resuspension of natural Pb in the near-bottom AABW layer changes Pb isotope signatures in the opposite direction as the vertical transport of anthropogenic Pb and this can prevent the latter to be observable, especially as both processes are

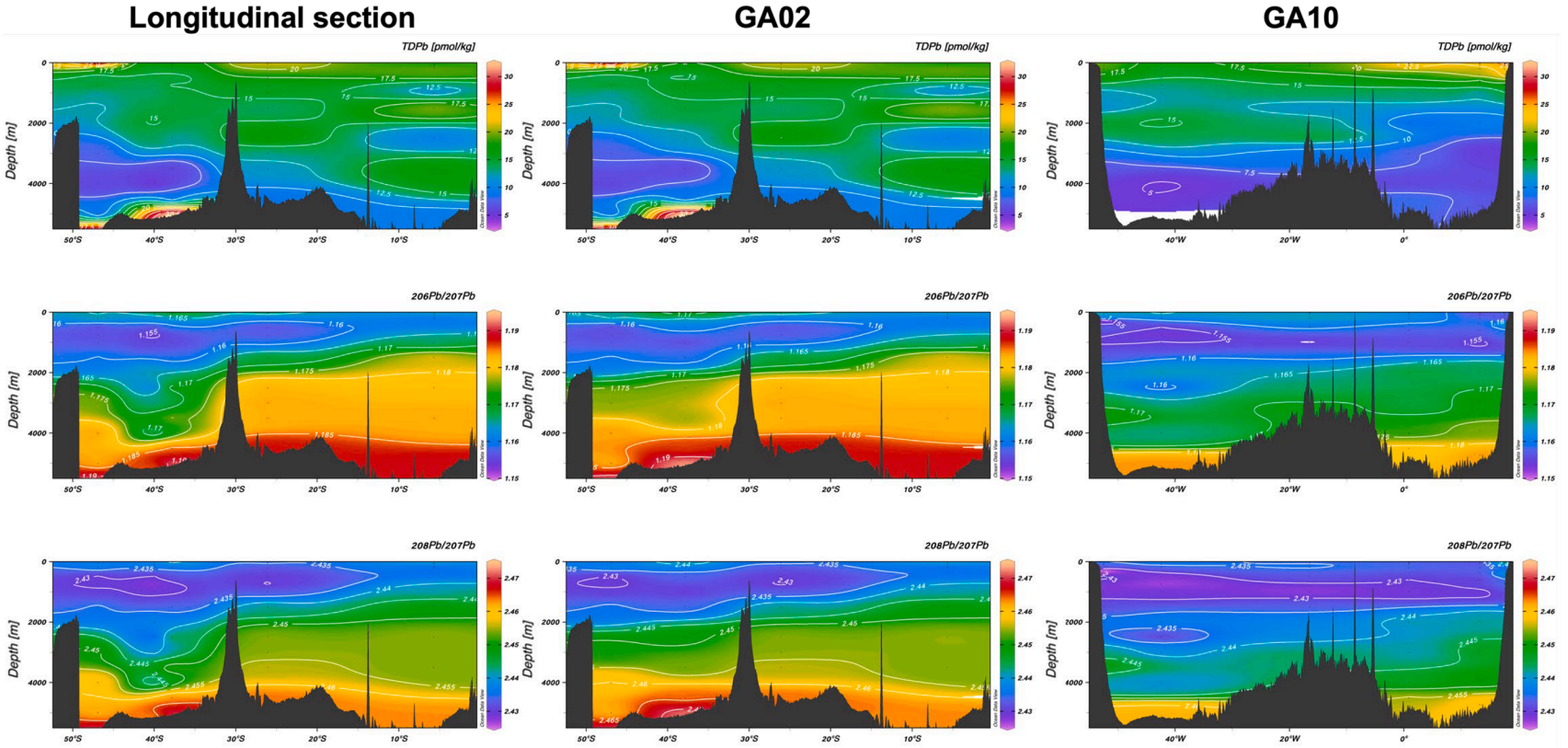

Fig. 7. Pb concentrations (top row), $^{206}Pb/^{207}Pb$ (middle row), and $^{208}Pb/^{207}Pb$ (bottom row) for the longitudinal, GA02 and GA10 (latitudinal) sections. Contour lines for each variable are plotted in white.

predominant in the western side of the basin.

Data from all depth profiles collected on cruise GA10 provide additional evidence of enhanced vertical transport of anthropogenic Pb by reversible scavenging in the western sector of the South Atlantic Ocean at ~40°S. Between 30 and 50°W, areas with lower $^{206}Pb/^{207}Pb$ and $^{208}Pb/^{207}Pb$ values than the surrounding water can be observed between 500 and 4000 m depth (Fig. 7). Interestingly, all samples collected below 2000 m on GA10 have lower Pb isotope ratios than their depth counterparts collected on GA02. This observation suggests that two mechanisms might be at play in determining the Pb isotope composition of seawater along the ~40°S section of the South Atlantic: 1) eastward transport at depth of the anthropogenic Pb isotope signature anomaly generated at the Brazil – Malvinas Confluence, and 2) downward (vertical) transport of anthropogenic Pb due to scavenging along the entire section, as suggested by the high chlorophyll-a concentration in the surface layer, although with a lesser extent in the eastern basin of the South Atlantic (Fig. 1B). As no direct measurements of SPM loads and particulate Pb isotope compositions in the water column are available, more data are needed to assess the extent of the role played by each of the two suggested mechanisms.

Aerosols were collected on GA10 and the Pb isotope data available for these samples are compatible with the suggested process of vertical transport, especially in the western side of the basin (Table S8, S9; Khondoker, 2014). Lead isotope compositions of bulk aerosols and aerosol leachates, which aim to represent the Pb released to rain and seawater following partial aerosol dissolution, display a similar spatial pattern to the GA10 surface seawater samples analysed in this study (Fig. S8). In general, aerosols show much more variable Pb isotope compositions (Table S9) than seawater samples from the mixed layer (Table 2). In the western South Atlantic, the Pb isotope ratios of the aerosols match within error those of all seawater samples collected in the water column, indicating that the aerosol Pb isotope signatures are compatible with those of intermediate and deep seawater samples (Fig. S8). In contrast, the data obtained for aerosols in the eastern South Atlantic show different systematics. Here, aerosol and seawater Pb isotope compositions are available for both the first (2010) and second (2012) leg of the GA10 cruise. While the bulk aerosol Pb isotope data are similar for the two legs, the mean Pb isotope compositions of the aerosol leachates show significant differences, with much lower values in 2010 than in 2012 (Table S9). This is reflected in the surface seawater Pb isotope compositions of samples collected at Stations 8_r and 6 in 2010, which have lower $^{206}Pb/^{207}Pb$ and $^{208}Pb/^{207}Pb$ ratios compared to samples collected in 2012 on the rest of the section (Fig. 3). However, based on these two profiles, the low Pb isotope ratios of the aerosols do not seem to have penetrated the water column, possibly because lower SPM loads in the eastern side of the South Atlantic (Browning et al., 2014) prevented efficient downward transport.

Overall, these observations and the results of the eOMP analysis suggest that vertical transport of anthropogenic Pb by marine particles in combination with reversible scavenging alter the advected Pb isotope signature in areas with high SPM loads. Where such processes are active, they can hence invalidate the use of Pb isotopes as transient tracers of water masses. As Pb isotopes have been extensively used as tracers of past ocean circulation (Frank, 2002), these findings may also have paleoceanographic implications. It is conceivable, for example, that in areas where SPM loads were high in the past, the sedimentary record of Pb isotope compositions might reflect the presence of vertical rather than advective Pb transport.

6. Conclusions

New Pb concentration and isotope composition data for 10 depth profiles collected in the South Atlantic Ocean on GEOTRACES cruises GA02 and GA10 are presented in this study. Lead concentrations decrease with depth, with the exclusion of two near-bottom samples from Stations 3 and 7 (GA02), where remobilisation of sedimentary Pb with a natural isotopic signature is detected. The $^{206}Pb/^{207}Pb$ and $^{208}Pb/^{207}Pb$ ratios display minima at ~1000 m, at the core of the AAIW, and then a progressive increase towards greater depths. Evidence is presented for vertical transport of anthropogenic Pb by reversible scavenging in the western side of the South Atlantic Ocean, where the two near-crossover stations of GEOTRACES cruises GA02 (Station 7) and GA10 (Station 18) show discrepancies in their Pb isotope composition depth profiles. These discrepancies are hypothesised to reflect different levels of suspended particles at the time of sampling. Lastly, Pb isotopes are found to be good tracers of water masses forming in the Southern Hemisphere, but not of NADW. Indeed, the latter shows significantly different Pb isotope signatures for the GA02 and GA10 sections between 2000 and 4000 m, which can be ascribed to vertical transport of more anthropogenic Pb at ~40°S, especially in the western South Atlantic. Our study hence provides the first evidence for vertical transport of anthropogenic Pb from surface waters to greater depths in the South Atlantic Ocean, consistent with findings in the Pacific Ocean (Lanning et al., 2023). As such, our findings suggest that caution must be used when Pb isotope ratios are used to trace water mass movements or ocean ventilation times on large scales, particularly in regions where processes such as reversible scavenging may have a significant impact on the marine biogeochemical cycling of Pb.

Funding

Arianna Olivelli was supported by the Natural Environment Research Council (NERC) (NE/S007415/1), as were Dominik Weiss, Tina van de Flierdt, and Mark Rehkämper (NE/H006095/1). Maeve Lohan was funded by NERC (NE/H004475/1). The GEOTRACES GA02 section cruises were made possible by the Netherlands Organization for Scientific Research (NWO) project grant 839.08.410. For the purpose of open access, the author has applied a Creative Commons Attribution (CC BY) license to any Author Accepted Manuscript version arising.

CRediT authorship contribution statement

Arianna Olivelli: Writing – review & editing, Writing – original draft, Visualization, Project administration, Investigation, Data curation. **Maxence Paul:** Investigation, Data curation. **Hui Xu:** Writing – review & editing. **Katharina Kreissig:** Writing – review & editing, Supervision, Resources, Methodology. **Barry J. Coles:** Supervision, Resources, Methodology. **Rebekah E.T. Moore:** Writing – review & editing, Supervision. **Luke Bridgestock:** Writing – review & editing. **Micha Rijkenberg:** Writing – review & editing. **Rob Middag:** Writing – review & editing. **Maeve C. Lohan:** Writing – review & editing. **Dominik J. Weiss:** Writing – review & editing, Project administration, Conceptualization. **Mark Rehkämper:** Writing – review & editing, Supervision, Project administration, Funding acquisition, Conceptualization. **Tina van de Flierdt:** Writing – review & editing, Supervision, Project administration, Funding acquisition, Conceptualization.

Declaration of competing interest

The authors declare that they have no known competing financial interests or personal relationships that could have appeared to influence the work reported in this paper.

Data availability

The data will be available via GEOTRACES. Code and results of the eOMP analysis will be available upon request.

Acknowledgements

Steven van Heuven is thanked for sharing his MATLAB code for the

eOMP analysis. We are grateful to Gideon Henderson for his efforts as Chief Scientist on GEOTRACES cruise GA10 and for coordinating the UK GEOTRACES consortium that carried out the work on the samples collected during the cruise. Gregory de Souza and Mark Baskaran are thanked for their useful comments throughout the review process.

Supplementary materials

Supplementary material associated with this article can be found, in the online version, at doi:10.1016/j.epsl.2024.118980.

References

Alleman, L.Y., Véron, A.J., Church, T.M., Flegal, A.R., Hamelin, B., 1999. Invasion of the abyssal North Atlantic by modern anthropogenic lead. Geophys. Res. Lett. 26 (10), 1477–1480. https://doi.org/10.1029/1999GL900287.

Azar, E., Piñango, A., Wallner-Kersanach, M., Kerr, R., 2021. Source waters contribution to the tropical Atlantic central layer: New insights on the Indo-Atlantic exchanges. In: Deep-Sea Research Part I: Oceanographic Research Papers, 168. https://doi.org/10.1016/j.dsr.2020.103450.

Bacon, M.P., Anderson, R.F., 1982. Distribution of thorium isotopes between dissolved and particulate forms in the deep sea. J. Geophys. Res.: Oceans 87 (C3), 2045–2056. https://doi.org/10.1029/jc087ic03p02045.

Bacon, M.P., Spencer, D.W., Brewer, P.G., 1976. 210Pb/226Ra and 210Po/210Pb Disequilibria in Seawater and Suspended Particulate Matter. Earth. Planet. Sci. Lett. 32, 277–296.

Bertinetti, S., Ardini, F., Vecchio, M.A., Caiazzo, L., Grotti, M., 2020. Isotopic analysis of snow from Dome C indicates changes in the source of atmospheric lead over the last fifty years in East Antarctica. Chemosphere 255. https://doi.org/10.1016/j.chemosphere.2020.126858.

Boyle, E.A., Lee, J.M., Noble, A.E., Moos, S., Carrasco, G., Zhao, N., Kayser, R., Zhang, J., Gamo, T., Obata, H., Norisuye, K., 2014. Anthropogenic lead emissions in the ocean: The evolving global experiment. Oceanography 27 (1), 69–75. https://doi.org/10.5670/oceanog.2011.80.

Bridgestock, L., Rehkämper, M., van de Flierdt, T., Paul, M., Milne, A., Lohan, M.C., Achterberg, E.P., 2018. The distribution of lead concentrations and isotope compositions in the eastern Tropical Atlantic Ocean. Geochim. Cosmochim. Acta 225, 36–51. https://doi.org/10.1016/j.gca.2018.01.018.

Browning, T.J., Bouman, H.A., Moore, C.M., Schlosser, C., Tarran, G.A., Woodward, E.M. S., Henderson, G.M., 2014. Nutrient regimes control phytoplankton ecophysiology in the South Atlantic. Biogeosciences. 11 (2), 463–479. https://doi.org/10.5194/bg-11-463-2014.

Chen, M., Boyle, E.A., Jiang, S., Liu, Q., Zhang, J., Wang, X., Zhou, K., 2023. Dissolved Lead (Pb) Concentrations and Pb Isotope Ratios Along the East China Sea and Kuroshio Transect—Evidence for Isopycnal Transport and Particle Exchange. J. Geophys. Res.: Oceans 128 (2). https://doi.org/10.1029/2022JC019423.

Chen, M., Boyle, E.A., Lee, J.M., Nurhati, I., Zurbrick, C., Switzer, A.D., Carrasco, G., 2016. Lead isotope exchange between dissolved and fluvial particulate matter: A laboratory study from the Johor River estuary. Philosoph. Trans. R. Soc. :Math., Phys. Eng. Sci. 374 (2081) https://doi.org/10.1098/rsta.2016.0054.

Chien, C.Te, Ho, T.Y., Sanborn, M.E., Yin, Q.Z., Paytan, A, 2017. Lead concentrations and isotopic compositions in the Western Philippine Sea. Mar. Chem. 189, 10–16. https://doi.org/10.1016/j.marchem.2016.12.007.

Chung, Y., Craig, H., 1983. 210Pb in the Pacific: the GEOSECS measurements of particulate and dissolved concentrations. Earth. Planet. Sci. Lett. 65, 406–432.

Craig, H., Krishnaswami, S., Somayajulu, B.L.K., 1973. 210Pb-226Ra: Radioactive disequilibrium in the deep sea. Earth. Planet. Sci. Lett. 17, 295–305.

Deng, F., Thomas, A.L., Rijkenberg, M.J.A., Henderson, G.M., 2014. Controls on seawater 231Pa, 230Th and 232Th concentrations along the flow paths of deep waters in the Southwest Atlantic. Earth. Planet. Sci. Lett. 390, 93–102. https://doi.org/10.1016/j.epsl.2013.12.038.

Dulaquais, G., Boye, M., Rijkenberg, M.J.A., Carton, X., 2014. Physical and remineralization processes govern the cobalt distribution in the deep western Atlantic Ocean. Biogeosciences. 11 (6), 1561–1580. https://doi.org/10.5194/bg-11-1561-2014.

Frank, M., 2002. Radiogenic isotopes: Tracers of past ocean circulation and erosional input. Rev. Geophys. 40 (1) https://doi.org/10.1029/2000RG000094, 1-1-1–38.

Galer, S.J.G., Abouchami, W., 1998. Practical application of lead triple spiking for correction of instrumental mass discrimination. Mineral. Mag. 491–492.

Garcia, C.A.E., Sarma, Y.V.B., Mata, M.M., Garcia, V.M.T., 2004. Chlorophyll variability and eddies in the Brazil-Malvinas Confluence region. Deep-Sea Res. Part II: Top. Stud. Oceanogr. 51 (1–3), 159–172. https://doi.org/10.1016/j.dsr2.2003.07.016.

Gardner, W.D., Jo Richardson, M., Mishonov, A.V., Biscaye, P.E, 2018. Global comparison of benthic nepheloid layers based on 52 years of nephelometer and transmissometer measurements. Prog. Oceanogr. 168, 100–111. https://doi.org/10.1016/j.pocean.2018.09.008.

GEOTRACES Intermediate Data Product Group, 2021. The GEOTRACES Intermediate Data Product 2021 (IDP2021). NERC EDS British Oceanographic Data Centre NOC.

Griffiths, A., Packman, H., Leung, Y.L., Coles, B.J., Kreissig, K., Little, S.H., Van De Flierdt, T., Rehkämper, M., 2020. Evaluation of optimized procedures for high-precision lead isotope analyses of seawater by multiple collector inductively coupled plasma mass spectrometry. Anal. Chem. 92 (16), 11232–11241. https://doi.org/10.1021/acs.analchem.0c01780.

Henderson, G.M., Maier-Reimer, E., 2002. Advection and removal of 210Pb and stable Pb isotopes in the oceans: A general circulation model study. Geochim. Cosmochim. Acta 66 (2), 257–272. https://doi.org/10.1016/S0016-7037(01)00779-7.

Hernández-Molina, F.J., Maldonado, A., Stow, D.A.V., 2008. Chapter 18 Abyssal Plain Contourites. Dev. Sedimentol. 60, 347–378. https://doi.org/10.1016/S0070-4571(08)00218-5.

Honeyman, B.D., Santschi, P.H., 1989. A Brownian-pumping model for oceanic trace metal scavenging: Evidence from Th isotopes. J. Mar. Res. 47, 951–992. https://elischolar.library.yale.edu/.

Kelly, A.E., Reuer, M.K., Goodkin, N.F., Boyle, E.A., 2009. Lead concentrations and isotopes in corals and water near Bermuda, 1780-2000. In: Earth and Planetary Science Letters, 283, pp. 93–100. https://doi.org/10.1016/j.epsl.2009.03.045.

Khondoker, R., 2014. Sources of Aerosols Over the South Atlantic Ocean. Imperial College London.

Komárek, M., Ettler, V., Chrastný, V., Mihaljevič, M., 2008. Lead isotopes in environmental sciences: A review. Environ. Int. 34 (4), 562–577. https://doi.org/10.1016/j.envint.2007.10.005.

Lanning, N.T., Jiang, S., Amaral, V.J., Mateos, K., Steffen, J.M., Lam, P.J., Boyle, E.A., Fitzsimmons, J.N., 2023. Isotopes illustrate vertical transport of anthropogenic Pb by reversible scavenging within Pacific Ocean particle veils. Proc. Natl. Acad. Sci. u S. a (23), 120. https://doi.org/10.1073/pnas.2219688120.

Lee, J.M., Boyle, E.A., Gamo, T., Obata, H., Norisuye, K., Echegoyen, Y., 2015. Impact of anthropogenic Pb and ocean circulation on the recent distribution of Pb isotopes in the Indian Ocean. Geochim. Cosmochim. Acta 170, 126–144. https://doi.org/10.1016/j.gca.2015.08.013.

Li, Z., Groeskamp, S., Cerovečki, I., England, M.H., 2022. The origin and fate of Antarctic intermediate water in the Southern Ocean. J. Phys. Oceanogr. 52 (11), 2873–2890. https://doi.org/10.1175/jpo-d-21-0221.1.

Middag, R., de Baar, H.J.W., Bruland, K.W., 2019. The relationships between dissolved zinc and major nutrients phosphate and silicate along the GEOTRACES GA02 Transect in the West Atlantic Ocean. Global. Biogeochem. Cycles. 33 (1), 63–84. https://doi.org/10.1029/2018GB006034.

Middag, R., de Baar, H.J.W., Bruland, K.W., van Heuven, S.M.A.C., 2020. The distribution of nickel in the west-Atlantic ocean, its relationship with phosphate and a comparison to cadmium and zinc. Front. Mar. Sci. 7 https://doi.org/10.3389/fmars.2020.00105.

Middag, R., van Heuven, S.M.A.C., Bruland, K.W., de Baar, H.J.W., 2018. The relationship between cadmium and phosphate in the Atlantic Ocean unravelled. Earth. Planet. Sci. Lett. 492, 79–88. https://doi.org/10.1016/j.epsl.2018.03.046.

Middag, R., van Hulten, M.M.P., Van Aken, H.M., Rijkenberg, M.J.A., Gerringa, L.J.A., Laan, P., de Baar, H.J.W., 2015. Dissolved aluminium in the ocean conveyor of the West Atlantic Ocean: Effects of the biological cycle, scavenging, sediment resuspension and hydrography. Mar. Chem. 177, 69–86. https://doi.org/10.1016/j.marchem.2015.02.015.

Mishonov, A.V., Gardner, W.D., Richardson, M.J., 2003. Remote sensing and surface POC concentration in the South Atlantic. Deep-Sea Res. Part II: Top. Stud. Oceanogr. 50 (22–26), 2997–3015. https://doi.org/10.1016/j.dsr2.2003.07.007.

Niedermiller, J., Baskaran, M., 2019. Comparison of the scavenging intensity, remineralization and residence time of 210Po and 210Pb at key zones (biotic, sediment-water and hydrothermal) along the East Pacific GEOTRACES transect. J. Environ. Radioact. 198, 165–188. https://doi.org/10.1016/j.jenvrad.2018.12.016.

Noble, A.E., Echegoyen-Sanz, Y., Boyle, E.A., Ohnemus, D.C., Lam, P.J., Kayser, R., Reuer, M., Wu, J., Smethie, W., 2015. Dynamic variability of dissolved Pb and Pb isotope composition from the U.S. North Atlantic GEOTRACES transect. Deep-Sea Res. Part II: Top. Stud. Oceanogr. 116, 208–225. https://doi.org/10.1016/j.dsr2.2014.11.011.

Nozaki, Y., Thomson, J., Turekian, K.K., 1976. The Distribution of 210Pb and 210Po in the Surface Waters of the Pacific Ocean. Earth. Planet. Sci. Lett. 32, 304–312.

Nozaki, Y., Zhang, J., Takeda, A., 1997. 210Pb and 210Po in the equatorial Pacific and the Bering Sea: the effects of biological productivity and boundary scavenging. Deep-Sea Res. II 44 (9–10), 2203–2220.

Olivelli, A., Murphy, K., Bridgestock, L., Wilson, D.J., Rijkenberg, M., Middag, R., Weiss, D.J., van de Flierdt, T., Rehkämper, M., 2023. Decline of anthropogenic lead in South Atlantic Ocean surface waters from 1990 to 2011: New constraints from concentration and isotope data. Mar. Pollut. Bull. 189 https://doi.org/10.1016/j.marpolbul.2023.114798.

Orsi, A.H., Smethie, W.M., Bullister, J.L., 2002. On the total input of Antarctic waters to the deep ocean: A preliminary estimate from chlorofluorocarbon measurements. J. Geophys. Res.: Oceans (8), 107. https://doi.org/10.1029/2001jc000976.

Pacyna, J.M., Pacyna, E.G., 2001. An assessment of global and regional emissions of trace metals to the atmosphere from anthropogenic sources worldwide. Environ. Rev. 9 (4), 269–298. https://doi.org/10.1139/er-9-4-269.

Paul, M., Bridgestock, L., Rehkämper, M., van de Flierdt, T., Weiss, D., 2015a. High-precision measurements of seawater Pb isotope compositions by double spike thermal ionization mass spectrometry. Anal. Chim. Acta 863 (1), 59–69. https://doi.org/10.1016/j.aca.2014.12.012.

Paul, M., van de Flierdt, T., Rehkämper, M., Khondoker, R., Weiss, D., Lohan, M.C., Homoky, W.B., 2015b. Tracing the Agulhas leakage with lead isotopes. Geophys. Res. Lett. 42 (20), 8515–8521. https://doi.org/10.1002/2015GL065625.

Planaj, D., Baskaran, M., 2024. Inventory-based evaluation of 210Po-210Pb-226Ra disequilibria in deep oceans and new insights on their utility as biogeochemical tracers: A global data synthesis of research over six decades. Earth. Sci. Rev. 252 https://doi.org/10.1016/j.earscirev.2024.104759.

Planchon, F.A.M., Van De Velde, K., Rosman, K.J.R., Wolff, E.W., Ferrari, C.P., Boutron, C.F., 2003. One hundred fifty-year record of lead isotopes in Antarctic snow from Coats Land. Geochim. Cosmochim. Acta 67 (4), 693–708. https://doi.org/10.1016/S0016-7037(00)01136-5.

Poole, R., Tomczak, M., 1999. Optimum multiparameter analysis of the water mass structure in the Atlantic Ocean thermocline. Deep-Sea Res. I 46, 1895–1921.

Richardson, M.J., Weatherly, G.L., Gardner, W.O., 1993. Benthic storms in the Argentine Basin. Deep-Sea Res. II 40 (4/5), 975–987.

Rigaud, S., Stewart, G., Baskaran, M., Marsan, D., Church, T., 2015. 210Po and 210Pb distribution, dissolved-particulate exchange rates, and particulate export along the North Atlantic US GEOTRACES GA03 section. Deep-Sea Res. Part II: Top. Stud. Oceanogr. 116, 60–78. https://doi.org/10.1016/j.dsr2.2014.11.003.

Rijkenberg, M.J.A., Middag, R., Laan, P., Gerringa, L.J.A., Van Aken, H.M., Schoemann, V., De Jong, J.T.M., De Baar, H.J.W., 2014. The distribution of dissolved iron in the West Atlantic Ocean. PLoS. One (6), 9. https://doi.org/10.1371/journal.pone.0101323.

Rudge, J.F., Reynolds, B.C., Bourdon, B., 2009. The double spike toolbox. Chem. Geol. 265 (3–4), 420–431. https://doi.org/10.1016/j.chemgeo.2009.05.010.

Rüth, C., Well, R., Roether, W., 2000. Primordial 3He in South Atlantic deep waters from sources on the Mid-Atlantic Ridge. Deep-Sea Res. I 47, 1059–1075.

Saito, M.A., Noble, A.E., Tagliabue, A., Goepfert, T.J., Lamborg, C.H., Jenkins, W.J., 2013. Slow-spreading submarine ridges in the South Atlantic as a significant oceanic iron source. Nat. Geosci. 6 (9), 775–779. https://doi.org/10.1038/ngeo1893.

Santoso, A., England, M.H., 2004. Antarctic intermediate water circulation and variability in a coupled climate model. J. Phys. Oceanogr. 34, 2160–2179.

Santoso, A., England, M.H., Hirst, A.C., 2006. Circumpolar Deep Water Circulation and Variability in a Coupled Climate Model.

Saraceno, M., Provost, C., Piola, A.R., 2005. On the relationship between satellite-retrieved surface temperature fronts and chlorophyll a in the western South Atlantic. J. Geophys. Res.: Oceans 110 (11), 1–16. https://doi.org/10.1029/2004JC002736.

Schlitzer, R., Usbeck, R., Fischer, G., 2004. Inverse modeling of particulate organic carbon fluxes in the South Atlantic. The South Atlantic in the late Quaternary: Reconstruction of Material Budgets and Current Systems, pp. 1–19.

Schlosser, C., Karstensen, J., Woodward, E.M.S., 2019. Distribution of dissolved and leachable particulate Pb in the water column along the GEOTRACES section GA10 in the South Atlantic. Deep-Sea Res. Part II: Top. Stud. Oceanogr. 148, 132–142. https://doi.org/10.1016/j.dsr.2019.05.001.

Sherrell, R.M., Boyle, E.A., Hamelin, B., 1992. Isotopic equilibration between dissolved and suspended particulate lead in the Atlantic Ocean: evidence from 210Pb and stable Pb isotopes. J. Geophys. Res. 97 (C7), 11257–11268. https://doi.org/10.1029/92jc00759.

Souza, A.G.Q.de, Kerr, R., Azevedo, J.L.L.de, 2018. On the influence of Subtropical Mode Water on the South Atlantic Ocean. J. Marine Syst. 185, 13–24. https://doi.org/10.1016/j.jmarsys.2018.04.006.

Stramma, L., England, M., 1999. On the water masses and mean circulation of the South Atlantic Ocean. J. Geophys. Res.: Oceans 104 (C9), 20863–20883. https://doi.org/10.1029/1999jc900139.

Talley, L., Pickard, G., Emery, W., Swift, J., 2011. Descriptive Physical Oceanography. Elsevier. https://doi.org/10.1016/C2009-0-24322-4.

Thomalla, S.J., Fauchereau, N., Swart, S., Monteiro, P.M.S., 2011. Regional scale characteristics of the seasonal cycle of chlorophyll in the Southern Ocean. Biogeosciences. 8 (10), 2849–2866. https://doi.org/10.5194/bg-8-2849-2011.

Tomczak, M., 1981. A multi-parameter extension of temperature/salinity diagram techniques for the analysis of non-isopycnal mixing. Prog. Oceanogr. 10, 147–171.

Tuerena, R.E., Ganeshram, R.S., Geibert, W., Fallick, A.E., Dougans, J., Tait, A., Henley, S.F., Woodward, E.M.S., 2015. Nutrient cycling in the Atlantic basin: The evolution of nitrate isotope signatures in water masses. Global. Biogeochem. Cycles. 29 (10), 1830–1844. https://doi.org/10.1002/2015GB005164.

Véron, A.J., Church, T.M., Flegal, A.R., 1998. Lead isotopes in the western north Atlantic: transient tracers of pollutant lead inputs. Environ. Res. 78, 104–111.

Véron, A.J., Church, T.M., Rivera-Duarte, I., Flegal, A.R., 1999. Stable lead isotopic ratios trace thermohaline circulation in the subarctic North Atlantic. Deep-Sea Res. II 46, 919–935.

von Blanckenburg, F., O'Nions, R.K., Hein, J.R., 1996. Distribution and sources of pre-anthropogenic lead isotopes in deep ocean water from Fe-Mn crusts. Geochim. Cosmochim. Acta 60 (24), 4957–4963.

Woodhead, J., 2002. A simple method for obtaining highly accurate Pb isotope data by MC-ICP-MS. J. Anal. At. Spectrom. 17 (10), 1381–1385. https://doi.org/10.1039/b205045e.

Wu, J., Rember, R., Jin, M., Boyle, E.A., Flegal, A.R., 2010. Isotopic evidence for the source of lead in the North Pacific abyssal water. Geochim. Cosmochim. Acta 74 (16), 4629–4638. https://doi.org/10.1016/j.gca.2010.05.017.

Wyatt, N.J., Milne, A., Woodward, E.M.S., Rees, A.P., Browning, T.J., Bouman, H.A., Worsfold, P.J., Lohan, M.C., 2014. Biogeochemical cycling of dissolved zinc along the GEOTRACES South Atlantic transect GA10 at 40°S. Global. Biogeochem. Cycles. 28 (1), 44–56. https://doi.org/10.1002/2013GB004637.

Xia, X., Hong, Y., Du, Y., Xiu, P., 2022. Three types of antarctic intermediate water revealed by a machine learning approach. Geophys. Res. Lett. (21), 49. https://doi.org/10.1029/2022GL099445.

Xie, R.C., Galer, S.J.G., Abouchami, W., Rijkenberg, M.J.A., De Jong, J., De Baar, H.J.W., Andreae, M.O., 2014. The cadmium-phosphate relationship in the western South Atlantic - The importance of mode and intermediate waters on the global systematics. Mar. Chem. 177, 110–123. https://doi.org/10.1016/j.marchem.2015.06.011.